Published in final edited form as:

Immunity. 2021 November 09; 54(11): 2547–2564.e7. doi:10.1016/j.immuni.2021.10.002.

Commensal *Cryptosporidium* colonization elicits a cDC1-dependent Th1 response that promotes intestinal homeostasis and restricts other infections

Emilie V. Russler-Germain[1], **Jisun Jung**[1], **Aidan T. Miller**[1], **Shannon Young**[1], **Jaeu Yi**[1], **Alec Wehmeier**[1], **Lindsey E. Fox**[1], **Kristen J. Monte**[1], **Jiani N. Chai**[1], **Devesha H. Kulkarni**[2], **Lisa J. Funkhouser-Jones**[3], **Georgia Wilke**[3], **Vivek Durai**[4], **Bernd H. Zinselmeyer**[4], **Rafael S. Czepielewski**[4], **Suellen Greco**[5], **Kenneth M. Murphy**[4], **Rodney D. Newberry**[2], **L. David Sibley**[3,*], **Chyi-Song Hsieh**[1,*,†]

[1]Department of Internal Medicine, Division of Rheumatology, Washington University School of Medicine, St. Louis, MO 63110, USA.

[2]Department of Internal Medicine, Division of Gastroenterology, Washington University School of Medicine, St. Louis, MO 63110, USA.

[3]Department of Molecular Microbiology, Washington University School of Medicine, St. Louis, MO 63110, USA.

[4]Department of Pathology, Division of Immunobiology, Washington University School of Medicine, St. Louis, MO 63110, USA.

[5]Division of Comparative Medicine, Washington University School of Medicine, St. Louis, MO 63110, USA.

Summary

Cryptosporidium can cause severe diarrhea and morbidity, but many infections are asymptomatic. Here, we studied the immune response to a commensal strain of *Cryptosporidium tyzzeri* (*Ct*-STL) serendipitously discovered when conventional type 1 dendritic cell (cDC1)-deficient mice developed cryptosporidiosis. *Ct*-STL was vertically transmitted without negative health effects in wild-type mice. Yet, *Ct*-STL provoked profound changes in the intestinal immune system, including induction of an IFNγ-producing Th1 response. T cell receptor sequencing coupled with *in vitro* and *in vivo* analysis of common Th1 TCRs revealed that *Ct*-STL elicited a dominant antigen-specific Th1 response. By contrast, deficiency in cDC1s skewed the *Ct*-STL CD4 T cell

*Correspondence: chsieh@wustl.edu and sibley@wustl.edu.
†Lead Contact

Author contributions: E.R.-G., C.-S.H., and L.D.S., conceived the project and/or designed the experiments. E.R.-G., J.J., A.T.M., S.Y., J.Y., A.W., L.E.F., K.J.M., J.N.C., D.H.K., L.F.-J., G.W., V.D., S.G., K.M.M., R.D.N., L.D.S., and C.-S.H. performed experiments, provided critical reagents, or analyzed data. B.Z. and R.S.C. contributed to setting up the luciferase experiment. E.R.-G. and C.-S.H. wrote the manuscript. All authors reviewed and edited the manuscript.

Declaration of Interests: The authors declare no competing interests.

response toward Th17 and regulatory T cells. Although *Ct*-STL predominantly colonized the small intestine, colon Th1 responses were enhanced and associated with protection against *Citrobacter rodentium* infection and exacerbation of dextran sodium sulfate and anti-IL10R-triggered colitis. Thus, *Ct*-STL represents a commensal pathobiont that elicits Th1-mediated intestinal homeostasis that may reflect asymptomatic human *Cryptosporidium* infection.

eTOC Blurb

Cryptosporidium are protozoan parasites that cause gastrointestinal illness in humans and animals worldwide. We identified a commensal strain of *Cryptosporidium tyzzeri* endemic in our mouse colony. This strain of *Cryptosporidium* does not cause disease in wild-type mice but changes the composition and function of the intestinal immune system.

Introduction

Cryptosporidium species are environmentally ubiquitous protozoan parasites that infect gastrointestinal epithelial cells of a broad range of animals (Fayer et al., 2010). Humans are mainly infected by *Cryptosporidium hominis* (Morgan-Ryan et al., 2002) and *Cryptosporidium parvum* (*Cp*) (Upton and Current, 1985). Infection starts with ingestion of oocysts, which contain 4 sporozoites that invade enterocytes and form parasitophorous vacuoles just below the apical enterocyte membrane. Asexual and then sexual development within enterocytes culminates in the generation of thick-walled, environmentally hardy oocysts that are excreted into the lumen to facilitate fecal-oral transmission.

Cryptosporidium is the fourth leading cause of death globally in children under the age of 5 (12.1%) (Collaborators, 2017), and is the second or third cause of diarrhea in in young children in Southeast Asia and Africa (Kotloff et al., 2019). Within the United States there are ~750,000 cases of cryptosporidiosis annually (Gharpure et al., 2019; Scallan et al., 2011). Cryptosporidiosis is also one of the original opportunistic infections characteristic of AIDS (Current et al., 1983). Moreover, therapies for cryptosporidiosis are limited, with only a single FDA-approved drug (nitazoxanide) that is ineffective in immunocompromised individuals and not approved in young children (Checkley et al., 2015). One issue for controlling transmission is that oocysts are resistant to bleach and other common disinfectants (Checkley et al., 2015). Thus, *Cryptosporidium* infection of humans remains an important health problem.

For many years, *Cryptosporidium* was thought to be a commensal (Flanigan and Soave, 1993). *Cryptosporidium* is now studied primarily as a pathogen due to its ability to cause human disease. One limitation of these studies is that mouse models typically rely on *Cp*, which naturally infects cows and humans but not wild-type (WT) mice (Upton and Current, 1985), thus requiring studies in immunocompromised mice such as IFNγ signaling-deficient (Chen et al., 1993a) or neonatal mice (Urban et al., 1996). A mouse-tropic species, *Cryptosporidium tyzzeri* (*Ct*, formerly mouse genotype I) (Morgan et al., 1999; Ren et al., 2012), infects the jejunum and ileum in mice and is closely related to *Cp* (Ren et al., 2012). Infection in wild mice is common with a worldwide distribution (Condlova et al., 2019; Osman et al., 2017b), and is reported to affect 2% of lab mice in China (Lv et al., 2009).

Adult mice shed *Ct* oocysts for 24–28 days post colonization, after which oocysts become undetectable. However, the mice remain infected as steroid administration at day 65 elicits oocyst shedding (Ren et al., 2012). A different strain of *Ct* isolated from wild mice from a farm (Sateriale et al., 2019) also infects adult C57BL/6 mice, which shed oocysts for up to 3 weeks. In this case, the oocysts are no longer detectable by qPCR after the initial infection.

We serendipitously discovered that our laboratory's mouse colony at Washington University in St. Louis has likely been colonized for years with a strain of *Ct* (*Ct*-STL) when conventional type 1 dendritic cell (cDC1)-deficient mice developed spontaneous cryptosporidiosis. Notably, the perspective of our study is different than studies that assessed *Ct* as an infection (Ren et al., 2012; Sateriale et al., 2019). In contrast to these reports, we found that *Ct*-STL acted like a commensal pathobiont, undergoing vertical transmission with colonization at weaning and oocyst shedding that persisted for the lifetime of the mouse without immunosuppression. As *Cryptosporidium* was detected in ~7% of animal rooms sampled in our building, this suggests that *Ct* may be common yet remain undetected in routine analyses of the microbiome given that such analyses tend to focus on prokaryotes through 16S rRNA sequencing. Thus, the immune system effects of *Ct* colonization may represent a major hidden variable in the study of gastrointestinal immune function.

Results

cDC1-deficient mice develop fulminant cryptosporidiosis

During the course of our studies of host:commensal interactions, we utilized *Irf8* +32 5'$^{-/-}$ mice that have a 149 base pair enhancer deletion in *Irf8* that efficiently eliminates cDC1s (Durai et al., 2019). Binding of BATF3 to this enhancer induces IRF8 expression in cDC1s, but does not affect IRF8 expression in other cell lineages. We bred *Irf8* +32 5'$^{-/-}$ mice to human Langerin-DTA (hLang^{DTA}) mice, which express diphtheria toxin (DTA) under the control of the human langerin promoter, to also delete CD103^{+} CD11b^{+} (double positive, DP) cDC2s in the mesenteric lymph nodes (MLN) (Welty et al., 2013). As neither of these cDC-subset-deficient strains were reported to develop spontaneous disease, we were surprised to observe that approximately 10% of homozygous *Irf8* +32 5'$^{-/-}$ mice failed to thrive and died between 5–20 weeks of age. hLang^{DTA} *Irf8* +32 5'$^{-/-}$ mice, which lack most CD103^{+} cDCs (Figure S1A), seemed more prone to this spontaneous illness, although still with variable penetrance.

Necropsy analysis of a sick hLang^{DTA} *Irf8* +32 5'$^{-/-}$ mouse revealed pancytopenia with low white blood cells (WBC), red blood cells (RBC), and platelets, as well as small secondary lymphoid organs and hyposplenism (Figure 1A–B). However, bone marrow histology only showed mild hypocellularity with reduced megakaryocytes (Figure 1C), which would not account for the profound pancytopenia observed. Notably, small intestine (SI) histology was pathognomonic for cryptosporidiosis (Figure 1C). Laboratory values such as low total protein were consistent with malabsorption secondary to cryptosporidiosis, which could also explain pancytopenia (Figure 1A). Thus, the presumptive cause of death of sick cDC1-deficient mice in our colony was fulminant cryptosporidiosis.

Ct-STL behaves like a commensal in WT mice

To characterize the species of *Cryptosporidium* in these mice, we analyzed parasite *Gapdh* (Huang et al., 2004) and *Gp60* genes (Xiao, 2010) by PCR amplification from fecal DNA. *Gapdh* sequencing revealed a high degree of similarity with *Ct*-UGA55 versus *Cp*-AUCP-1 (Sateriale et al., 2019; Wilke et al., 2019) (Figure 1D). Parasite *Gp60* also showed the greatest similarity with *Ct* amongst the *Cryptosporidium* genus (Figure S1B). Based on these genetic similarities, we refer to the strain in our St. Louis colony as *Ct*-STL.

We suspected that *Ct*-STL originated from WT Foxp3$^{\text{IRES-GFP}}$ mice bred in our colony for a decade. To quantify oocyst shedding, we performed flow cytometry (Barbosa et al., 2008) using a commercial antibody used to detect *Cryptosporidium* in human clinical samples (Crypt-a-Glo), which we found cross reacts with *Ct*-STL (Figure S2A). We found that our WT mice shed *Ct*-STL oocysts, while mice recently purchased from Charles River (CR) or Jackson (JAX) Laboratories showed no evidence of *Cryptosporidium*, consistent with monitoring and exclusion of this organism in their facilities (Figure 2A). Histological analysis of jejunums from our WT mice revealed characteristic signs of *Cryptosporidium* parasites in the brush border of epithelial cells (Figure 2B). Some strains in our colony were negative for *Ct*-STL, suggesting that it does not always spread between cages within a barrier facility. *Cryptosporidium* was not unique to our colony, however, as a PCR survey of air dust swabbed from the exhaust plenums of individually ventilated cage racks revealed that 7 out of 101 rooms in our facility were positive. Although we cannot ascertain when we acquired *Ct*-STL, our impression based on these data is that *Ct*-STL has been endemic in our colony for many years.

The presence of *Ct*-STL in multiple strains implies that it is vertically transmitted and maintained in the colony. To determine at what point during ontogeny WT mice become naturally colonized with *Ct*-STL, we compared oocyst numbers in the colon luminal contents of mice pre-weaning (14–21 days old) and post-weaning (3–6 weeks old) by flow cytometry. We also utilized *Ct*-STL *Gapdh* qPCR from fecal DNA to improve sensitivity of detection, with the caveat that this is not specific for DNA within oocysts. These analyses revealed that oocyst shedding became easily detectable around weaning (Figure 2C), likely via the fecal-oral route. Additionally, 9- to 13-month-old WT mice from our colony shed oocysts, albeit at low levels compared to younger mice (Figure 2D). These data are consistent with our conclusion that *Ct*-STL has been present in our colony for years, as transient infection would limit opportunities for vertical and horizontal transmission and likely lead to elimination from our colony.

To determine the infectious dose of *Ct*-STL, we generated a *Ct*-STL oocyst preparation free of bacterial constituents by treating cecal and colon contents from infected mice with 40% bleach, which rendered aerobic bacterial colony forming units (CFUs) undetectable. In contrast to *Cp*, which requires upward of 10^6 oocysts to cause transient infection of WT mice (Theodos et al., 1997), transfer of as few as 250 *Ct*-STL oocysts at weaning infected WT mice (Figures 2E and S2B). In fact, 250, 4×10^3, and 2.5×10^4 oocysts all produced similar levels of colonization over time as measured by oocyst shedding, which remained stable for many weeks before decreasing at week 12 post-infection (Figures 2E and S2B). However, qPCR analysis revealed an inverse relationship between initial *Ct*-STL dose and

Ct-STL DNA in stool at 12 weeks (Figure S2B), suggesting that large inoculations may trigger increased sterilizing immunity. Based on these data, we transferred 4×10^3 oocysts in *Cryptosporidium*-free mice at weaning to mimic homeostatic vertical infection unless otherwise noted. FACS-purified oocysts from this preparation also transferred *Ct*-STL, suggesting that oocysts alone were sufficient for colonization (data not shown). These data show that *Ct*-STL has a low infectious dose in WT mice and persists over 3 months, consistent with observations from naturally-colonized mice.

We next assessed whether *Ct*-STL colonization affected the overall health of the animal. Colonization with *Ct*-STL at weaning did not affect weight gain over 7 weeks (Figure 2F). 1 year after colonization, *Ct*-STL was still detected in the stool of these mice (Figure S2C). Colonization with *Ct*-STL also did not affect fecundity or cause signs of diarrhea or increased intestinal permeability (Figures 2G–H and S2D). Therefore, in contrast to other *Ct* strains (Ren et al., 2012; Sateriale et al., 2019), *Ct*-STL acts less like a pathogen and more like a commensal.

Both innate and adaptive immunity are required to limit *Ct*-STL

IFNγ signaling is important in the control of *Cp* in mice (Chen et al., 1993b; Pollok et al., 2001; Tessema et al., 2009). Consistent with these observations, we found that anti-IFNγ antibody treatment increased *Ct*-STL oocyst shedding by 2 weeks, an effect also seen with *Cp* (Chen et al., 1993a) (Figure S3A). Additionally, *Ifngr1*$^{-/-}$ mice lost weight starting 1–2 weeks after *Ct*-STL colonization, with some mice succumbing to infection over the 4 week observation period (Figure S3B). Taken together, these data support a pivotal role for IFNγ signaling for controlling *Ct*-STL.

Multiple innate and adaptive cell types secrete IFNγ, including NK, ILC1, NKT, CD4$^+$ T, and CD8$^+$ T cells (Cortez and Colonna, 2016; Schoenborn and Wilson, 2007). *Cryptosporidium* control requires adaptive immunity (Current et al., 1983; Sateriale et al., 2019; Tandel et al., 2019). To assess whether T and B cells are necessary for the control of *Ct*-STL, we colonized *Rag1*$^{+/-}$ and *Rag1*$^{-/-}$ littermates with *Ct*-STL and tracked stool oocysts. Differences in oocyst shedding began at 3–4 weeks post-colonization, when oocyst shedding decreased in *Rag1*$^{+/-}$ mice (Figures 3A and S3C). Notably, *Rag1*$^{-/-}$ mice colonized with *Ct*-STL did not appear ill or lose weight (Figure 3B). Histologic analysis of jejunums revealed that *Rag1*$^{-/-}$ mice had decreased villus height and villus:crypt length ratio indicative of crypt hyperplasia, and a trend toward more *Ct*-STL organisms per villus than *Rag1*$^{+/-}$ littermates (Figures 3C and S3D). Thus, these data from mice deficient in T and B cells highlight the low pathogenicity of *Ct*-STL and confirm that adaptive immunity is required to limit *Ct*-STL infection.

As *Rag1*$^{-/-}$ mice only showed a defect in late control of *Ct*-STL colonization, we wondered whether components of innate immunity also participate in control of *Ct*-STL. We depleted NK and ILC cells with weekly anti-NK1.1 and anti-Thy1.2 antibodies, respectively. *Rag1*$^{-/-}$ mice shed significantly more *Ct*-STL oocysts with depletion of innate lymphocytes (Figure 3D). Altogether, these data highlight the critical role of type I immunity from both innate and adaptive immune cells for the control of *Ct*-STL.

To better understand the requirement for cDC1s to prevent fulminant cryptosporidiosis, we asked whether *Ct*-STL colonization alters cDC subsets. At 1 week post-colonization, cDC1 frequencies were unchanged and the percentage of MLN migratory DP cDC2s was slightly decreased (Figure S3E). We also asked whether *Ct*-STL induces a signal for Th1 development, IL-12 (Hsieh et al., 1993) using *Cryptosporidium*-free IL-12p40^{YFP} mice. At 1 week post-colonization, IL-12p40^{YFP} was selectively induced in a small fraction of cDC1s in the small intestine lamina propria (SILP) (Figures 3E and S3F). IL-12p40^{YFP} was not enhanced in cDC1s in the MLN, although the baseline frequency of expression was substantial (Figure S3F). Macrophages also secrete IL-12 (Cooper and Khader, 2007), but induction of IL-12p40^{YFP} expression was not observed in SILP macrophages (Figure S3F). The observation that IL-12p40 was only induced in cDC1s provides an explanation for why cDC1-deficient mice were susceptible to *Ct*-STL (Figure 1).

The induction of IL-12p40 in cDC1s suggests that *Ct*-STL induces an adaptive Th1 response, consistent with responses to other *Cryptosporidium* (Urban et al., 1996). Colonization of *Cryptosporidium*-free IFNγ^{YFP} IL17A^{GFP} Foxp3$^{IRES\text{-}Thy1.1}$ triple reporter mice with *Ct*-STL revealed increased frequency and mean fluorescent intensity (MFI) of IFNγ^{YFP} expression in CD4^{+} T cells in the SILP (Figure 3F) with similar trends in the proximal MLN (pMLN, all but distal MLN; Figure S3G). Additionally, the increase in CD4^{+} T cell IFNγ corresponded with a loss of IL-17A^{GFP+} Th17, but not Foxp3$^{IRES\text{-}Thy1.1+}$ regulatory T (Treg) cells (Figures 3F and S3G). Consistent with an adaptive immune response to *Ct*-STL, increased CD4^{+} T cell numbers were also observed in the SILP (Figure S3G). CD8^{+} T cells play a role in *Cp* clearance in mice, although not as important a role as CD4^{+} T cells (McDonald et al., 1994). While CD3ε $^{+}$ CD4^{-}T cells, which included both CD8^{+} T cells but also a small fraction of other T cell subsets such as γδ T cells, were increased in numbers in the SILP by *Ct*-STL colonization, *Ct*-STL induced a decrease in IL17A^{GFP} but no change in IFNγ^{YFP} expression in CD4^{-} T cells (Figures S3H–I). Thus, in contrast to other commensals, *Ct*-STL elicits a strong adaptive Th1 response.

Ct-STL induces an antigen-specific Th1 response

T cell responses after *Ct*-STL colonization could be specific to *Cryptosporidium* vs. other gut antigens (Hand et al., 2012). To address the question regarding TCR specificity, we analyzed the T cell receptor α (TCRα) repertoire (Table S1) of fixed TCRβ transgenic mice treated with anti-IFNγ to increase parasite burden (Figure S3A). Here, we used CXCR3 as a surrogate for Tbet-expressing Th1 cells in the MLN (Groom, 2019). A unique TCR was designated by its TRAV designation and CDR3 amino acid sequence.

Comparison of TCRα repertoires using non-metric multidimensional scaling (NMDS) of Bray-Curtis distances revealed that the effector T (Teff) cell repertoires in the MLN and SILP underwent substantial changes with *Ct*-STL infection in comparison with the Treg TCR repertoire (Figure 4A). The differences in TCR repertoire were greater between Treg and Teff cells (axis 1 of NMDS) than the effect of *Ct*-STL (axis 2 of NMDS), suggesting that convergence of the Treg and Teff TCR repertoires does not occur, in contrast to DSS plus anti-IL-10R induced colitis (Chai et al., 2017). The top Teff clones in *Ct*-STL infected mice in the presence of anti-IFNγ were virtually absent in control mice (Figures 4B and

S4A, Table S2). By contrast, the most abundant Treg TCRs in *Ct*-STL mice were present at relatively high frequencies in control mice.

Based on early data, we selected 2 clones, RG1 and RG2, for analysis of antigen specificity as they were found in high frequencies in Teff subsets (Figures 4B–C, S4A). RG1 and RG2 TCRα clones were retrovirally transduced into hybridoma cells expressing the fixed TCRβ chain and an NFAT-GFP reporter for T cell activation (Chai et al., 2017; Lathrop et al., 2011). We found that both RG1 and RG2 were activated by Flt3L-induced DCs presenting SI epithelial cell preparations from *Ct*-STL infected mice as well as *Cp* oocysts (Figure 4D). The antigens recognized by these TCRs likely differ as RG1 preferentially reacted to the SI epithelial preparation, whereas RG2 exhibited stronger reactivity to the *Cp* oocysts, consistent with differences in the CDR3 amino acid composition of the TCRs tested (Figures 4C–D). As controls, we observed that SI epithelial preparations from uninfected mice did not activate RG1 or RG2. Also, *Ct*-STL or *Cp* antigen preparations did not activate a *Helicobacter*-reactive CT6 hybridoma, arguing against antigen non-specific mechanisms of T cell activation. Later, we also discovered that RG3 was reactive to *Cp* oocysts and confirmed that all 3 TCRs recognized antigen via conventional MHC Class II presentation (Figure S4B). Taken together, these data demonstrate that 3 common Teff TCRs that expanded with *Ct*-STL infection in mice treated with anti-IFNγ are specific to *Cryptosporidium* antigens.

We next asked whether these TCRs react to *Ct*-STL in WT colonized mice at homeostasis. We retrovirally transduced RG1 or RG2 into TCliαβ T cells (Lathrop et al., 2011), which expressed the original TCRβ chain and an αβ-TCR reactive to an irrelevant foreign peptide (human CLIP). RG1 or RG2 transduced T cells transferred *in vivo* were barely recoverable from control mice but were readily detected in *Ct*-STL colonized mice and underwent extensive cell division based on Cell Trace Violet (CTV) dilution 1 week after transfer (Figures 4E and S4C). These data demonstrate that *Ct*-STL antigens are constitutively acquired by antigen presenting cells (APCs) and presented to $CD4^+$ T cells during homeostatic colonization of WT mice.

We also asked if RG1 and RG2 T cells could develop into peripheral Treg (pTreg) cells *in vivo* under homeostatic conditions, akin to the adaptive T cell response to pathobionts of the *Helicobacter* genus (Chai et al., 2017; Xu et al., 2018). Although the process of retroviral transduction requires *in vitro* activation, we are able to maintain the ability of the transferred cells to undergo pTreg cell differentiation (Chai et al., 2017). We observed that neither RG1 nor RG2 differentiated into Treg cells in 1 week when transferred early or late after *Ct*-STL colonization, and instead increased expression of CXCR3 in the MLN, which is suggestive of Th1 development (Groom, 2019) (Figures 4F–G and S4D). We confirmed that RG1 and RG2 T cells increased expression of Tbet and had minimal FoxP3 expression using intracellular staining (Figures 4H and S4E–F). In summary, these data suggest that RG1 and RG2 TCRs undergo Th1 development to *Ct*-STL *in vivo* under homeostatic conditions.

Ct-STL colonization alters the small intestine TCR repertoire at homeostasis

As the above T cell studies utilized retroviral transduction or anti-IFNγ treatment, the results may not mimic naïve T cell differentiation and miss pTreg cell selection to *Ct*-

STL. We therefore analyzed the TCRα repertoire at homeostasis using triple reporter IFNγ^{YFP} IL17A^{GFP} Foxp3$^{IRES\text{-}Thy1.1}$ mice. IL17A^{GFP+} TCR repertoires were not analyzed due to variably low cell numbers, as *Ct*-STL induces a loss of these cells (Figure 3F). NMDS of Bray-Curtis distances revealed that SILP Teff subsets, including Th1, and IFNγ^{YFP-} IL17A^{GFP-} double negative (Teff-DN) cells, underwent shifts as a result of *Ct*-STL colonization (PERMANOVA p-values: SILP Th1=0.006, SILP Teff DN=0.106, SILP Treg=0.593, MLN Th1=0.149, MLN Teff-DN=0.078, MLN Treg=0.435) (Figures 4A, 5A). Treg TCR repertoires were less affected by *Ct*-STL (Figure S5A).

To further assess the changes induced by *Ct*-STL colonization on specific T cell subsets, we compared the frequencies of TCR clones that were present in both control and *Ct*-STL colonized mice. SILP Th1, but not Teff-DN or Treg TCR, clones underwent substantial decreases in frequency in *Ct*-STL-colonized mice (Figure 5B). We interpret this to mean that the antigenic landscape for Teff-DN or Treg T cells are not as dramatically altered by *Ct*-STL, whereas the relative frequencies of Th1 cells that recognize non-*Ct*-STL antigens are diminished either by *Ct*-STL specific Th1 expansion or via alteration of cDC presentation of those antigens.

As another approach for identifying TCRs associated with *Ct*-STL infection, we used gradient boosted models (GBM), a tree based machine learning algorithm related to random forest. Using the effector TCR datasets (Teff-DN and Th1) from the SILP, MLN and colon lamina propria (cLP) at homeostasis, we optimized the parameters to achieve an AUC of 0.99 (Figure 5C). The TCRs with highest relative influence (Figure 5C) concur with the assessment that RG1, RG2, and RG3 are common TCRs that distinguish the homeostatic effector TCR repertoire during *Ct*-STL colonization.

We also looked at the top TCR clones by average frequency induced by *Ct*-STL colonization. The top 9 out of 10 *Ct*-STL SILP Th1 TCR clones, including RG1 and RG2, were absent in control mice and in Treg cells (Figures 5D and S5B, Table S3). By contrast, the majority of the top SILP Treg TCR clones in *Ct*-STL were also present in control mice (Figure 5D). Many of the top SILP Th1 TCRs were also found in the Teff-DN subset (Figures S5B–C), suggesting that only a portion of T cells of the same specificity are actively synthesizing IFNγ, or that these TCRs are present in other effector T cell phenotypes. The top MLN Th1 and Teff-DN TCRs during homeostasis were not as uniformly absent in control mice (Figure S5D), indicating a more limited impact of *Ct*-STL in the MLN consistent with the NMDS (Figure 5A). TCR repertoire analysis of individual TCRs using DESeq2 also showed that RG1, RG2, and RG3 were mostly increased in the Th1 and Teff-DN but not Treg cell populations in *Ct*-STL-colonized versus control mice ($p_{adj} < 0.05$) (Figure S5E). Thus, *Ct*-STL colonization during homeostatic conditions elicits primarily a Th1-type effector, and not Treg, cell response, suggesting that pTreg cell selection is not an important mechanism by which host:commensal tolerance is achieved for C*t*-STL.

cDC1s are important for *Ct*-STL control and Th1 differentiation

To confirm that the fulminant cryptosporidiosis observed in cDC1-deficient mice was due to *Ct*-STL, we rederived hLang^{DTA} *Irf8* +32 5'$^{-/-}$ mice to be *Cryptosporidium*-free via *in vitro*

fertilization. cDC1-deficient mice colonized with *Ct*-STL at weaning shed increased oocysts (Figure 6A). Loss of DP cDC2s in hLang^{DTA} mice did not impact oocyst shedding (Figure 6A). Thus, cDC1s, but not DP cDC2s, are required for control of *Ct*-STL.

We wondered whether colonization of rederived cDC1-deficient mice would recapitulate the disease we observed in cDC1-deficient mice in our colony, partially fulfilling Koch's postulates. Over the course of 12 weeks after *Ct*-STL colonization at weaning, 2/20 (10%) *Irf8* +32 5'$^{-/-}$ mice vs 0/15 *Irf8* +32 5'$^{+/-}$ mice perished. Weight was maintained in the majority of cDC1-deficient mice, suggesting that fulminant cryptosporidiosis was a stochastic event – consistent with our initial observations in *Irf8* +32 5'$^{-/-}$ mice (Figures 1 and 6B). Rederived cDC1-deficient mice that were not colonized with *Ct*-STL showed no signs of illness and did not die prematurely (data not shown). Histologic analysis of surviving cDC-deficient mice showed cDC1-deficient mice had significantly more *Ct*-STL organisms per villus and higher epithelial scores due to villus epithelial dysplasia but otherwise comparable villus and crypt properties (Figures 6C and S6A). From these observations, we conclude that the morbidity and mortality observed in a subset of our original cDC1-deficient mice was due to fulminant cryptosporidiosis from *Ct*-STL.

Altered T cell development in cDC1-deficient mice is one explanation for the severity of *Ct*-STL-mediated disease observed in *Irf8* +32 5'$^{-/-}$ mice relative to *Rag1*$^{-/-}$ mice. For example, genetic regulation of Th1 vs Th2 responses results in dramatically different outcomes to *Leishmania major* infection (Sadick et al., 1990; Scott et al., 1988). We therefore analyzed RG1 after transfer into *Ct*-STL colonized, cDC-deficient mice. RG1 recovery was increased in the SILP of cDC1-deficient mice, consistent with increased *Ct*-STL antigen burden (Figure S6B). Notably, the frequency of RG1 FoxP3^{+} Treg cells was increased in 4/10 cDC1-deficient mice (Figure 6D and S6C). Additionally, Tbet^{+} Th1 generation of RG1 was diminished in cDC1-deficient mice, which was associated with skewing toward other Teff subsets: RORγt^{+} Th17 and GATA3^{+} Th2 cells (Figures 6E–F and S7D–E). With the exception of Treg cells in the MLN, RG1 differentiation mirrored the changes in polyclonal CD4^{+} T cell phenotype in cDC-deficient mice (Figure 6D–F and Figure S6C–E), suggesting that RG1 may be representative of the *Ct*-STL specific response. These shifts in *Ct*-STL-specific T cell differentiation from Th1 to Treg, Th2, and Th17 cells in cDC1-deficient mice may promote loss of immune control to *Ct*-STL.

In contrast, no changes in RG1 or polyclonal T cell development were observed in DP cDC2-deficient mice (Figures 6D–F and S7C–E). RG1 recovery was decreased in the MLN of hLang^{DTA} mice lacking DP cDC2s, indicating a role for this cDC subset in antigen presentation (Figure S6B). Deficiency of both cDC1s and DP cDC2s marginally increased the differentiation of RG1 into FoxP3^{+} Treg and RORγt^{+} Th17 cells versus cDC1 deficiency alone, but decreased the differentiation of GATA3^{+} Th2 cells (Figure 6D–F and Figure S6C–E). Thus, DP cDC2s contribute to the presentation of *Ct*-STL antigens and in the absence of cDC1s, are observed to promote Th2, but not Th1, differentiation.

Homeostatic *Ct*-STL induces colon Th1 responses and facilitates immunity to pathogens

In humans, *Cp* infection predominantly affects the jejunum and ileum (Leitch and He, 2012). To establish the extent to which *Ct*-STL colonizes different segments of the gastrointestinal

tract, we performed qPCR of *Ct*-STL *Gapdh* on the intestinal epithelial cell preparations of the duodenum, jejunum, ileum, and colon of *Ct*-STL colonized mice. We found that while *Ct*-STL DNA was highest in the ileum followed by the jejunum, *Ct*-STL DNA was detectable in duodenum epithelial preparations (Figure 7A). While the presence of DNA does not necessarily indicate productive infection, these data indicate the *Ct*-STL can be found throughout the SI.

As *Ct*-STL colonization alters T cell responses in SI, we wondered whether T cell tolerance to food antigens is altered. pTreg cell generation to oral OVA is blocked by SI infections (Bouziat et al., 2017; Esterhazy et al., 2019). In *Ct*-STL colonized mice, OT-II pTreg cell differentiation was unaffected (Figures S7A–B). Furthermore, *Ct*-STL colonization did not lead to a difference in inflammation with subsequent subcutaneous OVA challenge (Figure S7C). Although OVA is absorbed along the entire length of the SI (Esterhazy et al., 2019; Kulkarni et al., 2020), OT-II pTreg differentiation is highest in the duodenal-draining LNs (Esterhazy et al., 2019). Thus, lower *Ct*-STL in the duodenum may be one reason that pTreg cell generation to a food antigen is spared (Figure 7A). Alternatively, *Ct*-STL colonization may not affect SI T cell differentiation to other antigens due to cDC microenvironment restricted T cell development.

Cryptosporidium primarily infects the small, but not large, intestine in humans (Current and Reese, 1986). Consistent with this, qPCR of *Ct*-STL from mouse colon epithelial cells was at or below the limit of detection (>150-fold lower than ileal epithelial cells) and histologic analysis of *Ct*-STL-colonized hLang^{DTA} *Irf8* +32 5'$^{-/-}$ mice showed *Ct*-STL parasites in SI but not colon epithelial cells (Figures 7A and S7D). Furthermore, tracking of RG1 localization using T cells that retrovirally express Akaluc luciferase (Iwano et al., 2018) transferred into *Rag1*$^{-/-}$ mice showed they preferentially localized to the SI, in contrast to colon *Helicobacter*-specific CT2 cells, which localized to the cecum and colon (Figure S7E) (Chai et al., 2017; Nutsch et al., 2016). Nevertheless, analysis of colon polyclonal T cells after *Ct*-STL colonization revealed that IFNγ^{YFP+} CD4^{+} T cells were also increased in the cLP with *Ct*-STL (Figure 7B), which was confirmed by qRT-PCR of *Ifng* and *Tbx21* (Figure 7C). *Ct*-STL colonization also resulted in slightly decreased frequencies of Treg and Th17 cells in the cLP and distal colon-draining MLN (dMLN) (Figures 7B and S7F). Thus, these data suggest that *Ct*-STL also affects the colon T cell population and skews it toward a Th1 response.

To determine which other colon cytokines are affected by *Ct*-STL, we performed multiplex cytokine analysis of whole colons after *Ct*-STL colonization. We found that both IL12p40 and RANTES (CCL5) were increased in *Ct*-STL-colonized mice (Figures 7D and S7G). RANTES can be induced by IFNγ (Liu et al., 2005) to recruit monocytes and activated T cells (Schall et al., 1990), and RANTES expression in the colon is strongly associated with inflammation, including exacerbation of DSS-colitis (Ajuebor et al., 2001; Elinav et al., 2011). Overall, these data suggest that *Ct*-STL induces pro-inflammatory cytokine mediators of both innate and adaptive immunity in the colon.

Colon *Ct*-STL-induced effects may be due to changes in the colon microbiome. We assessed changes in bacterial communities using 16S rRNA sequencing and analysis of amplicon

sequence variants (ASVs) (Callahan et al., 2016). Colonization with *Ct*-STL minimally decreased species diversity (Shannon index) but shifted bacterial composition as assessed by PERMANOVA ($p = 0.001$) or NMDS (Figure S7H–I). *Ct*-STL colonization induced an increase in the frequency of *Prevotellaceae* at the expense of *Lachnospiraceae* (Figure S7J–K), the latter of which are producers of short chain fatty acids that are associated with the expansion of Treg cells (Arpaia et al., 2013; Furusawa et al., 2013; Smith et al., 2013). Additionally, increases in *Prevotellaceae* induce RANTES expression in colon epithelial cells (Elinav et al., 2011), possibly by stimulation of TLRs and NOD1/2 (Berube et al., 2009; Vaughan et al., 1991). However, study of the interaction of *Ct*-STL and microbiota is complicated, as treatment with broad-spectrum antibiotics increased *Ct*-STL oocyst shedding by 100–1000-fold (Figure S7L), consistent with previous *Cryptosporidium* studies (Charania et al., 2020). These data demonstrate that *Ct*-STL colonization can both alter and be altered by the composition of the colon microbiome in WT mice.

The alterations in gut bacteria by *Ct*-STL suggest that increased colon Th1 cells could be generated to commensal antigens. Analysis of the top cLP Th1 TCR clones revealed overlap with SILP Th1 TCR sequences (Figure 7E, Table S4), and included the *Ct*-STL specific TCRs RG1, RG2, and RG3 (Figures 4C–D and S4B). We tested 4 additional cLP Th1 TCRs (LA1–4) *in vitro* for reactivity to *Cryptosporidium* as well as *Ct*-STL-negative colon stool contents. Although LA1–4 did not react to stool antigens, this experiment does not exclude TCR recognition of luminal antigens that are in large particles or found at low concentration. However, we did discover that LA3 was reactive to *Cp* oocysts (Figure 7F). Together, the *Ct*-STL specific TCRs RG1, RG2, RG3, and LA3 made up a substantial fraction of the Th1 TCR repertoire in SILP and cLP tissues (Figure 7G). Additionally, RG1 T cells transferred into *Ct*-STL colonized mice expressed $IFN\gamma^{YFP}$ in the cLP at similar frequencies as RG1 cells recovered from the SILP, albeit with lower MFI (Figure 7H). In contrast, RG1 cells recovered from the spleen, peripheral (p)LNs, and MLN did not express $IFN\gamma^{YFP}$ (Figure 7H). RG1 cells recovered from the SILP and cLP fully diluted CTV, while RG1 recovered from the pLN, spleen, and MLN, some of which may represent recirculating cells, underwent fewer cell divisions (Figure 7H). Thus, these data indicate that the increase in colon Th1 cells with *Ct*-STL is driven, in large part, by the presence of *Ct*-STL specific T cells that are activated by *Ct*-STL antigens that are presented in the colon.

Finally, we asked whether *Ct*-STL affects colon immune function. We first assessed whether *Ct*-STL protects against *Citrobacter* (*C.*) *rodentium*, which infects the cecum and colon. For these experiments, we used strains of C3H (HeNCrl and HeOuJ) mice, which are more susceptible to *C. rodentium* than C57BL/6 mice (Vallance et al., 2003). Consistent with the role for type I immunity in *C. rodentium* infection (Bry et al., 2006; Shiomi et al., 2010; Spahn et al., 2008), we observed that colonization with *Ct*-STL decreased lethality (Figures 7I). Analysis of *C. rodentium* colony forming units (CFUs) from stool at early timepoints revealed that a subset of *Ct*-STL colonized mice had decreased CFUs at day 4 compared to control mice (Figure 7I). We also tested whether *Ct*-STL colonization modulated colon inflammation after treatment with DSS drinking water plus anti-IL10R antibody (Chai et al., 2017). As would be predicted from other studies where increased RANTES expression exacerbates DSS-colitis (Elinav et al., 2011), *Ct*-STL colonization was associated with increased lethality and colon injury in this model (Figures 7J). Thus,

these data all suggest that although *Ct*-STL colonization primarily occurs in the SI, *Ct*-STL induces clear functional changes in the colon immune system that may be due to a combination of IFNγ-expressing *Ct*-STL specific colon T cells, increased innate cytokines, and changes to the colon microbiome.

Discussion

The serendipitous discovery of a *Cryptosporidium* commensal pathobiont in our colony (*Ct*-STL) was revealed by spontaneous illness in cDC1-deficient mice. *Ct*-STL may have a very different infection profile compared to other *Ct* strains isolated from "wild" mice. These "wild" *Ct* strains induce robust immunity in laboratory mice, which stop shedding oocysts 2–3 weeks after infection (Ren et al., 2012; Sateriale et al., 2019), whereas WT C57BL/6 mice shed *Ct*-STL oocysts for months. Although a direct functional and genomic comparison between these strains is required to establish the pathogenic vs commensal "nature" of *Ct* strains and exclude variables such as *Ct* dose and host microbiota, we suspect that *Ct*-STL has low pathogenicity and is adapted to be a commensal in C57BL/6 mice. It is also important to note that although *Ct*-STL acts as a commensal in our mouse colony, it remains possible that malnutrition, exposure to other pathogens, or alterations in background microbiota may result in morbidity from commensal *Cryptosporidium*. Despite the great amount of work focused on the bacterial microbiota, parasites such as *Ct*-STL and *Tritrichomonas* (Chudnovskiy et al., 2016) may play a much greater role in dictating host:commensal immunity than previously appreciated, contributing to different results between labs and even between strains within a lab.

Our observation that *Ct*-STL elicits strong changes in the $CD4^+$ T cell compartment is consistent with existing knowledge of *Cryptosporidium* infections. First, cryptosporidiosis in humans is associated with low $CD4^+$ T cell counts in AIDS patients (Current et al., 1983; Petersen, 1992). Second, infection with "wild" *Ct* leads to persistent oocyst shedding over 6 months in $Rag1^{-/-}$ and athymic $Foxn1^{nu}$ mice (Sateriale et al., 2019). Finally, mice that lack MHC Class II, but not Class I, are susceptible to *Cp* infection (Aguirre et al., 1994). Although other immune cells likely contribute, $CD4^+$ T cells appear to be the most important immune cell subset for the control of *Cryptosporidium* infection.

Nonetheless, we were surprised to observe that *Ct*-STL, as a single commensal species, could cause such a dramatic induction of antigen-specific Th1 responses. The first reason is that a Th1 response to commensals has not been described, although other responses are reported. For example, segmented filamentous bacteria induce non-pathogenic Th17 cells (Ivanov et al., 2009), *Helicobacter*–pTreg cells (Chai et al., 2017; Xu et al., 2018), and *Akkermansia*–a mixed Th1, Th17, Treg, and Tfh cell response (Ansaldo et al., 2019). A colon Th1 and Th17 response is observed with *Tritrichomonas* parasites, although antigen specificity has not been examined (Chudnovskiy et al., 2016; Escalante et al., 2016).
A second reason is that Th1 responses are thought to portend inflammation and tissue destruction and not maintenance of homeostasis. One hypothesis is that *Ct*-STL may induce IL-10 producing Tr1 cells, which are also seen during *Toxoplasma* infection (Jankovic et al., 2007), and may be more important than Treg cells for maintaining tolerance in the SI (Roncarolo et al., 2018).

Homeostasis during *Ct*-STL colonization is dependent on cDC1-mediated type 1 immunity, consistent with previous reports. cDC1s are an important source of IL-12 for Th1 development in *Toxoplasma gondii* infection (Mashayekhi et al., 2011), which we also observed for *Ct*-STL. In addition, *Batf3*-mutant mice deficient in cDC1s (Hildner et al., 2008) are more susceptible to *Cp* infection (Potiron et al., 2019). However, adult *Batf3*$^{-/-}$ mice clear *Cp* within a week, which may reflect differences between *Cryptosporidium* species or residual mucosal cDC1s in the gut of *Batf3*$^{-/-}$ mice that can be expanded by infection (Mashayekhi et al., 2011; Tussiwand et al., 2012). Although all cDC1-deficient mice had increased shedding of *Ct*-STL oocysts, not all cDC1-deficient mice succumbed to cryptosporidiosis. The variables that influence infection severity are still unclear. Additionally, the specific mechanisms by which cDC1s, and not cDC2s, recognize *Cryptosporidium* and induce IL-12 remain to be elucidated.

Interestingly, we were still able to recover RG1 T cells from CD103^{+} cDC-deficient mice, suggesting that other APCs are capable of presenting *Ct*-STL antigens. One unexpected effect of cDC1-deficiency was that a fraction of *Ct*-STL specific RG1 T cells underwent pTreg cell differentiation. We hypothesize that cDC1s encountering *Ct*-STL provide a dominant signal such as IL-12 that prevents pTreg cell generation by other cDC subsets. Nonetheless, it remains unknown why cDC2s would facilitate pTreg cell selection to *Ct*-STL with the loss of cDC1s, and whether the ratio of pTreg to Th1 cell selection to *Ct*-STL could precipitate fulminant cryptosporidiosis.

Another unexpected finding is that *Ct*-STL's geographical impact extends well past the site of infection in the SI and also induces a Th1 response in the colon. There are several potential mechanisms for increased colon Th1 cells, including *Ct*-STL effects on the microbiota, colon epithelium, or innate immune milieu. However, our data showing that a substantial fraction of colon Th1 cells are *Ct*-STL specific and express IFNγ suggest that these T cells reencounter antigen in the colon acquired from either low level infection of colon epithelial cells or colon sampling of antigens present in the fecal stream. Increased Th1 cells in the colon was associated with increased resistance to colon infection by *Citrobacter* and susceptibility to injury by DSS plus anti-IL-10R treatment. Increased IFNγ may "pre-arm" innate cells such as macrophages to resist infection, akin to that seen with latent gamma-herpes virus-mediated protection against *Listeria* (Barton et al., 2007). Alternatively, IFNγ may induce the release of antimicrobial defenses from colon epithelium, as is seen for SI Paneth cells (Farin et al., 2014), or act directly on colon epithelial cells to alter homeostasis (Kominsky et al., 2014; Nava et al., 2010).

Study of the immune response to commensal *Ct*-STL may be relevant to human disease. In the United States, *Cryptosporidium* is typically thought of as a pathogen of periodic small outbreaks, but it is often endemic in the developing world (Checkley et al., 2015), where malnourished children have increased *Cryptosporidium* infection associated with more severe diarrheal illness (Mondal et al., 2012). However, there are likely commensal or pathobiont strains that infect humans, as different strains of *Cp* and *Cryptosporidium hominis* produce varying clinical manifestations from severe diarrhea to asymptomatic infection (Cama et al., 2008). In addition, the prevalence of chronic asymptomatic *Cryptosporidium* colonization of humans may be underappreciated, as typical methods of

detection are not sensitive and qPCR methods are not routinely utilized (Heine et al., 1984; Kuhls et al., 1992; Mead et al., 1991). Even in the United States, it is estimated that less than 1% of *Cryptosporidium* infections are diagnosed (Scallan et al., 2011). Finally, recent reports from Lebanon and Poland suggest that the presence of *Cryptosporidium* convey a 3 to 11-fold increased risk for colon adenocarcinoma (Osman et al., 2017a; Sulzyc-Bielicka et al., 2018). This is intriguing in light of our observation that *Ct*-STL increases susceptibility to colon injury, which can facilitate tumorigenesis (Terzic et al., 2010). Thus, *Ct*-STL may provide a useful murine model for understanding asymptomatic *Cryptosporidium* infection in human disease and the role of type 1 immunity in host:commensal tolerance.

Limitations of the Study

This study describes a strain of *Cryptosporidium* with characteristics of a commensal organism in mice. However, comparative studies using other mouse strains as well as studies in humans will be required to generalize these findings. We found that cDC1s are important for preventing Th17 and pTreg cell development to *Cryptosporidium*, but it remains unproven whether skewed T cell development and reduced IL-12 or IFNγ production in cDC1-deficient mice causes fulminant cryptosporidiosis. Finally, the notion that *Cryptosporidium* can markedly affect adaptive immunity in the colon will require future studies with other organisms to determine if this is a general phenomenon of small intestinal infections.

STAR METHODS

RESOURCE AVAILABILITY

Lead contact—Further information and requests for resources and reagents should be directed to and will be fulfilled by the lead contact, Chyi-Song Hsieh (chsieh@wustl.edu).

Materials availability—*Ct*-STL oocysts and TCR expression plasmids are available upon request.

Data and code availability—TCR and 16S rRNA sequencing data have been deposited at European Nucleotide Archive (ENA) and are publicly available as of the date of publication. Accession numbers are listed in the key resources table. This paper does not report original code. Any additional information required to reanalyze the data reported in this paper is available from the lead contact upon request.

EXPERIMENTAL MODEL AND SUBJECT DETAILS

Animal breeding and experiments were performed in a specific pathogen-free animal facility using protocols approved by the Washington University Institutional Animal Care and Use Committee (protocol #20–0036). Mice were maintained negative for the following agents: mouse hepatitis virus, Sendai virus, Theiler's murine encephalomyelitis virus, reovirus, ectromelia virus, pneumonia virus of mice, rotavirus, lymphocytic choriomeningitis virus, minute virus of mice, k virus, polyoma virus, mouse cytomegalovirus, mouse adenovirus, mouse parvovirus, *Mycoplasma pulmonis*, *Clostridium piliforme*, *Streptococcus pneumoniae*, *Bordetella bronchiseptica*, *Streptobacillus moniliformis*, *Corynebacterium*

kutscheri, *Salmonella species*, *Citrobacter rodentium*, fur mites, and pinworms. Mice were housed up to 5 per cage in autoclaved individually ventilated caging (NexGen, Allentown, NJ), with corncob bedding (The Andersons, Maumee, OH). Mice were fed ad lib irradiated rodent chow (LabDiet 5053WU, PMI Nutrition, St Louis, MO) and provided autoclaved municipal water in bottles. The mice were maintained on a 12:12 hour light cycle. Room temperature was maintained between 20–23° C and humidity between 30–70%. Littermates were used for all comparisons of genetic strains and *Ct*-STL colonization experiments unless noted otherwise. *Irf8* +32 5'$^{-/-}$ (149 bp deletion) (Durai et al., 2019) mice were a gift from K. Murphy (Wash.U.). Human Langerin-DTA mice (hLang^{DTA}) mice were a gift from D. Kaplan from U.Minn. (Kaplan et al., 2005). *Rag1*$^{-/-}$ (#002216), OT-II (#004194), Foxp3$^{IRES\text{-}GFP}$ (#006772), IL-17A$^{IRES\text{-}GFP}$ (#18472), p40$^{IRES\text{-}YFP}$ (#015864), *Ifngr1*$^{-/-}$ (#003288), and C3H/HeOuJ (#000635) mice were obtained from The Jackson Laboratory (JAX). IFN$\gamma^{IRES\text{-}YFP}$ "Great" mice (Reinhardt et al., 2009) were a gift from R. Locksley (University of California, San Francisco). TCli TCRβ *TCR*$\alpha^{+/-}$ and TCli TCR$\alpha\beta$ mice were previously described (Solomon and Hsieh, 2016; Wong et al., 2000). *Foxp3*$^{IRES\text{-}Thy1.1}$ mice were a gift from A. Rudensky (Memorial Sloan Kettering Cancer Center). C3H/HeNCrl (#025) were obtained from Charles River Laboratories. Ly5.1 and Ly5.2 mice from Charles River Laboratories were analyzed as wild-type mice. Both male and female mice were used for experiments with the exception of WT CR Ly5.1, Ly5.2, and C3H/HeNCrl mice, which were all male.

METHOD DETAILS

MLN and intestine lymphocyte isolation—For cDC analyses, dMLN or pMLN were dissociated in RPMI-Enzyme, containing 5% bovine calf serum, penicillin and streptomycin, 1 mM sodium pyruvate, non-essential amino acids, 50 μM beta-mercaptoethanol, 65.8 μg/ml collagenase VIII (Sigma # C2139), and 0.2 U/ml dispase (Thermo Fisher # CB-40235), for 45 minutes at 37°C with continuous stirring. Small intestine and colon lamina propria cells were isolated by performing 4, 12-minute washes in 5 mM EDTA in HBSS, shaking at 140 rpm at 37°C. Intestines were cut into small pieces and incubated in RPMI-Enzyme for 2 hours, shaking at 140 rpm at 37°C. Cells were filtered through a 100 μm filter before staining for FACS analysis with an FACSAria IIu (Becton Dickinson).

Intestine histology—Luminal contents were removed, and intestines flushed with 10% (v/v) formalin and fixed in 'swiss rolls' in cassettes in 10% (v/v) formalin overnight at room temperature (RT). Cassettes were washed and left in 70% ethanol at 4°C until paraffin embedding, cutting, and staining with H&E by Histology Consultation Services, Inc. (http://www.histocs.com). 5 continuous villus and crypt pairs in the same plane of section from the middle of the small intestine were imaged per slide using a ThermoFisher EVOS FL Auto Imaging System. Villus height and width, crypt depth and width, goblet cells per villus and crypt pair, mitoses per crypt, *Ct*-STL organisms per villus, and epithelial were quantified in a blinded fashion using ImageJ. For epithelial score (max 14), points were assigned for villus epithelial separation or sloughing (0=none, 1=cell separation from villus tip of 1–2 out of 5 villi evaluated, 2=cell separation from villus tip of 3–5 out of 5 villi evaluated, 3=denuded villus tips, 4=denuded villus tips with fibrin and/or inflammatory exudate), villus epithelial dysplasia (0=none, cells well aligned in monolayer, 1=cytoplasmic

basophilia with high nuclear:cytoplasmic ratio, 2=mild, multifocal epithelial disorganization, 3=regional moderate epithelial malalignment, 4=marked regional malalignment with cell piling), villus epithelial attenuation (0=none, epithelium are uniformly tall and columnar-shaped, 1=multifocal cuboidal- shaped epithelium, 2=regional-multiregional cuboidal shaped-epithelium, 3=flattened villus epithelium), and degree of crypt branching (0=none, 1=1–2 branches observed for 1–2 out of 5 crypts evaluated, 2=1–2 branches observed for 3–5 out of 5 crypts evaluated, 3=greater than 2 branches within 1 or more crypts out of 5 crypts evaluated) (Sateriale et al., 2019). Quantifications were averaged for each slide.

qPCR and sequencing of *Cryptosporidium* DNA—Quick-DNA Fecal/Soil Microbe Prep Kit (Zymo) was used to isolate DNA from terminal pellets. qPCR was carried out with Luminaris Color HiGreen qPCR Master Mix (ThermoFisher K0391) using a LightCycler 480 (Roche). For qPCR, *Cryptosporidium*-specific *Gapdh* was amplified with the primer pairs: F 5'-AAGGACTGGAGAGCAGGAAG −3' and R 5'-CCATACCTGTGAGCTTTCCA-3' (Wilke et al., 2018). Ct values were compared to *Cp* DNA corresponding to a known quantity of oocysts to calculate fecal *Ct*-STL oocyst equivalents. For Sanger sequencing of *Gapdh*, forward 5'-CGGTTTCGGACGTATTGGT-3', 5'-GACCCAGCAGAAATCCCATG;−3' and reverse 5'-TCCCTTCATTGGACCATTGGA-3', 5'-TGAAGCAACATAAACGGCGA-3' primers were used for *Ct*-STL and *Cp*-AUCP-1. For Sanger sequencing of *Gp60*, forward 5'-ATAGTCTCCGCTGTATTC-3' (AL3531) and reverse 5'-GGAAGGAACGATGTATCT-3' (AL3535) primers were used (Stensvold et al., 2014). Reference sequences were obtained from NCBI and CryptoDB and were aligned using MUSCLE in MegAlign (v16, DNASTAR) with Gap Penalty 25, Tamura-Nei distance, and pairwise gap removal with other options at the default setting; and plotted using ggtree (v2.1) in R. Quantification of *Ct*-STL DNA in intestinal epithelial cell preparations was performed from 6-week-old CR B6 mice, 3 weeks after gavage with 4×10^3 *Ct*-STL oocysts. Murine *Trac* qPCR was used to control for input DNA quantity. intestines were washed 4 times in PBS to remove stool. Duodenum, jejunum, and ileum were isolated based on the first 25%, middle 50%, and last 25% of SI (Esterhazy et al., 2019). Colon included the cecum. Intestines were incubated for 20-minutes in 5 mM EDTA in HBSS with 5% bovine calf serum, shaking at 140 rpm at 37°C. Intestines were removed, and the epithelial cells in suspension were filtered through a 100 μm filter and pelleted. DNA was isolated using DirectPCR Lysis Reagent (Viagen #301-C) and qPCR for *Ct*-STL *Gapdh* was performed as described above. ΔCt values were calculated using *Trac* qPCR to quantify epithelial cell input for each sample (primers: forward 5'-TTGAGCCAGGAGGAGACTTC-3' and reverse 5'-ATCAATGTGCCGAAAACCAT-3').

***Cryptosporidium* oocyst flow cytometry—**Terminal pellets were resuspended at 50 mg/ml in 5 mM EDTA in PBS. Pellets were vortexed for 20 minutes at 4°C, sonicated for 4 minutes, and passed through a 70 μM filter. CountBright Absolute Counting Beads (2.5 μl ThermoFisher #C36950) were added to 25 μl of filtrate, incubated for 20 minutes in 200 μl 5 mM N-acetyl-cysteine (Sigma) on ice. Samples were washed twice with PBS and blocked >20 minutes to overnight in 20% FBS in PBS on ice, stained with DAPI and 1:1000 and 20x Crypt-a-Glo (Waterborne #A400FLR) for 30 minutes, washed, and analyzed

by flow cytometry. Limit of specific detection was determined by pooling flow cytometry data for 82 known *Cryptosporidium*-free samples and calculating the 95% probability by negative binomial distribution that <2 oocyst events are detected in the average number of CountBright beads analyzed per sample.

***Ct*-STL repository—**Colon contents were harvested from *Rag1*$^{-/-}$ mice one week after gavage with stool from *Ct*-STL vertically infected *Irf8* +32 5'$^{-/-}$ mice. *Rag1*$^{-/-}$ mice were also treated with 1 mg/ml ampicillin, 1 mg/ml neomycin, and 0.5 mg/ml vancomycin in drinking water and 250 μg anti-IFNγ blocking antibody clone H22 (Leinco #I-438) for 2 days before infection. Feces were resuspended in cold sterile PBS by vortexing. Large debris was pelleted by slow spin at 200 rpm for 5 minutes at 4°C and the supernatant was transferred to a new tube. 100% bleach was added to the supernatant to a final concentration of 40%, incubated on ice for 10 minutes, and then washed 3 times with cold sterile PBS by centrifugation at 15,000 RPM. Oocysts in the sample were quantified by FACS analysis, stored at 4°C, and checked to ensure zero bacterial growth on aerobic LB plates at 37°C. Unless noted otherwise, for *Ct*-STL colonization experiments, mice were gavaged at weaning or 3.5 weeks of age with 200 μl PBS or 4×10^3 *Ct*-STL oocysts in 200 μl PBS.

Analysis of fecal water weight, SI transit velocity, and FITC uptake—Terminal fecal pellets were immediately collected in a pre-weighed Eppendorf tube, weighed again, and dried overnight at 80°C in open tubes. Pellets and tubes were re-weighed. The percentage of water in feces was obtained from the ratio of dry/pre-baked to fresh pellet weights. For SI transit velocity, mice were gavaged with red dye and the velocity of gastrointestinal transit was calculated by measuring the distance traveled in the small intestine over 30 minutes. The total GI transit time was determined by the amount of time after which the red dye was excreted in stool pellets. FITC-dextran 44mg/100g weight (Sigma #FD4) intestinal uptake in the serum was assessed as described at 4 hours (Gupta and Nebreda, 2014).

TCR sequencing and repertoire analysis—MLN and SILP CXCR3$^{+/-}$ Teff cells (CD4$^+$ Vβ6$^+$ CD44^{hi} CD62L^{lo} Foxp3$^-$) and Treg cells (CD4$^+$ Vβ6$^+$CD44^{hi} CD62L^{lo}Foxp3$^+$) were sorted from TCli TCRβ Foxp3$^{IRES\text{-}GFP}$ TCRα$^{+/-}$ or TCli TCRβ Foxp3$^{Thy1.1}$ IFNγ^{YFP} IL-17A^{GFP} *Tcra*$^{+/-}$ mice using a FACSAria IIu. TCRα DNA synthesis from sorted cells was performed as described (Chai et al., 2017). Amplification was performed using a multiplex PCR as described in Table S1. MiSeq TCR sequencing data of T cell populations from individual mice were analyzed via dada2 (v1.14) (Callahan et al., 2016) to identify amplicon sequence variants and reduce noise due to sequencing errors. TCR sequences were parsed as before to identify the TRAV and CDR3 amino acid sequence (Chai et al., 2017), which together are used to designate a unique TCR. TCR frequencies were calculated by dividing read counts for an individual TCR by the total reads in a sample. TCR repertoires were analyzed in R using phyloseq (v1.32), DESeq2 (v.1.28), and GBM (v2.1). Each GBM iteration was trained with a random 75% of the samples and tested against the remaining 25%, optimizing the variables n.min, interaction depth, and bag fraction for AUC. The final data represents the average of 400 iterations for relative influence of each TCR, and 100 iterations of each sample for prediction (25% of time as

test subset). Heatmaps are representative of TCR frequency averages from individual mice and TCRs selected for inclusion in heatmap analyses were present in at least 2 mice in the population being analyzed.

T cell hybridoma stimulation—T cell hybridoma cells expressing GFP under a minimal NFAT promoter (Ise et al., 2010) were retrovirally transduced with TCRα chains of interest as previously described (Chai et al., 2017; Lathrop et al., 2011). Hybridoma cells (1.5×10^4) were cultured with splenic CD11c$^+$ DCs (5×10^4) expanded *in vivo* with Flt3-ligand B16 melanoma cells in 200 μl D10 (200 μl complete DMEM (Thermo Fisher #SH3008101) with 10% FBS, Glutamax, 50 μM beta-mercaptoethanol, 1 mM sodium pyruvate, 10 mM HEPES, non-essential amino acids, and penicillin and streptomycin) in 96-well flat bottom plates with indicated concentrations of antigens for 40 hours at 37°C. TCRβ$^+$ cells were analyzed for GFP expression by FACS. Where noted, 50 μg/ml soluble anti-CD3ε (BioXCell BE0001–1) or 20 μg/ml MHC Class II blocking antibody (BioXCell BE010). was added to cultures.

Cryptosporidium* and other antigen preparations—Cp* oocyst antigen was prepared as previously described for vaccination (Wilke et al., 2019). For small intestine epithelial antigen preparations, Charles River mice were treated to enhance infection with 250 μg anti-IFNγ blocking antibody clone H22 (Leinco #I-438) and placed on 1 mg/ml ampicillin, 1 mg/ml neomycin, and 0.5 mg/ml vancomycin drinking water for one week. Mice were either gavaged with control PBS or 4×10^3 *Ct*-STL repository oocysts. Small intestine epithelial cells were isolated by a 12-minute wash in 5 mM EDTA in HBSS, shaking at 140 rpm at 37°C, filtered through a 40 μm filter, and then washed with sterile PBS. Stool antigens were prepared by collecting total colon luminal contents from *Ct*-STL negative TCli TCRβ Foxp3$^{Thy1.1}$ IFNγ^{YFP} IL-17A^{GFP} mice. Antigen samples were resuspended in sterile PBS, autoclaved, and filtered through a 37 μM filter. Stool antigens were also spun at 2000 rpm for 2 minutes to remove large particles; supernatant was used for antigen stimulation. Protein concentration was quantified by Bradford Assay.

Transduction and analysis of *Ct*-STL-specific TCRs in vivo—24 well plates were coated with 10 μg/ml anti-CD3ε (BioXCell BE0001–1) overnight at 4°C. Plates were washed out with PBS, and plated with 5×10^5 to 1.5×10^6 naïve (CD4$^+$Foxp3$^-$CD25$^-$CD44^{lo}CD62L^{hi}) T cells FACS sorted from TCli TCRαβ Foxp3$^{IRES\text{-}GFP}$ *Rag1*$^{+/-}$ Tg or TCli TCRβ Foxp3$^{Thy1.1}$ IFNγ^{YFP} IL-17A^{GFP} *Tcra*$^{+/-}$ mice in D10 in Th0 conditions (1 μg/ml anti-CD28 (BioXcell #BE0015–1), 10 μg/ml anti-TGFβ (BioXcell #BE0057), 5 μg/ml anti-IL-12 (BioXCell #BE0052), 5 μg/ml anti-IFNγ (BioXCell #BE0054), 5 mg/ml anti-IL4 (BioXCell #BE0045)). TCRα chain IRES-Thy1.1 retroviral transduction was performed as described (Hsieh et al., 2004) using TransIT-293 (Thermo Fisher #MIR2700). Transduced cultures were left to rest in Th0 media for ~66 hours. Foxp3$^-$ TCRα-transduced Thy1.1+ cells were sorted by FACS and 2×10^4 sorted cells were retro-orbitally injected into each host for *in vivo* analysis unless otherwise specified. Cells were stained with CTV (Thermo Fisher #C34571) in some experiments. Transferred cells were identified as CD4$^+$ Vβ6$^+$ Thy1.1$^+$. For transcription factor staining experiments,

10^5 cells were injected per mouse to increase recovery. Transcription factors were stained using the Foxp3/Transcription Factor Staining Buffer Set (Thermo Fisher #00–5523-00).

Bioluminescence Imaging—TCli TCRαβ Foxp3$^{IRES\text{-}GFP}$ *Rag1*$^{+/-}$ Tg mice were transduced with RG1 and CT2 TCRα chain P2A-Akaluc (Iwano et al., 2018)-expressing retroviruses in Th0 conditions as described above. 10^6 FACS-sorted RG1- or CT2-expressing cells were retro-orbitally-injected into *Rag1*$^{-/-}$ mice that had been gavaged with either 4×10^3 *Ct*-STL oocysts or *Helicobacter typhlonius*-containing stool 3 weeks prior. *In vivo* bioluminescence imaging was performed ten days later on an IVIS 50 (PerkinElmer, Waltham, MA; Living Image 4.3.1, 1 minute exposures, 4 bin, FOV12cm, f/stop1, open filter). Mice were injected intraperitoneally with AkaLumine-HCl (5mg in PBS;Sigma, St. Louis, MO) and imaged 5 minutes later using isoflurane anesthesia (2% vaporized in O2). Total photon flux (photons/sec) was measured from the abdomen using Living Image 2.6.

16S rRNA Sequencing—Fecal DNA was purified via column (Zymogenetics), and used in triplicate PCR of the bacterial V4 hypervariable region of 16S rRNA using barcoded primers described previously (Caporaso et al., 2011). PCR products were sequenced using the Illumina MiSeq platform (2×250-bp paired-end reads), and ASVs and taxonomy including species designations if possible (silva 1.32) determined by dada2 (Callahan et al., 2016). ASV data were analyzed by phyloseq (v1.32), vegan (v2.4), and DESeq2 (v.1.28) in R (3.6)

***In vivo* Antibody Treatment, Oral Tolerance, Colon Cytokine Analysis, *Citrobacter rodentium* Infection, DSS + anti-IL10R Treatment, and Antibiotic Treatment—**Where indicated, mice were treated IP with weekly 250 μg anti-IFNγ blocking antibody clone H22 (Leinco #I-438), 250 μg H22 isotype control clone PIP (Leinco #P-376), 500 μg anti-Thy1.2 clone 30H12 (BioXCell #BE0066), 500 μg 30H12 IgG2b isotype control clone LTF-2 (BioXCell #BE0090), 200 μg anti-NK1.1 clone PK136 (BioXCell #BE0036), or 200 μg PK136 isotype control IgG2a clone C1.18.4 (BioXCell #BE0085). Mice were colonized with 4×10^3 *Ct*-STL or gavaged with PBS at 3.5 weeks of age. Functional studies were performed 3 weeks later. Colon polyclonal CD4$^+$ T cells were analyzed by qPCR using the primers *Ifng*-forward 5'-TCCACATCTATGCCACTTGAG-3', *Ifng*-reverse 5'-CTGAGACAATGAACGCTACACA-3', *Tbx21*-forward 5'-CAACAACCCCTTTGCCAAAG-3', and *Tbx21*-reverse 5'-TCCCCCAAGCAGTTGACAGT-3'. For oral tolerance, mice were gavaged with 50 mg of OVA (Sigma #A5503) on day 1 and 2. Naïve CD4$^+$ CD25$^-$ Foxp3$^-$ CD44^{lo} CD62L^{hi} OT-II cells were sorted and 5×10^4 cells were injected per mouse on day 2. OT-II cells were analyzed from MLNs on day 8. For delayed type hypersensitivity (DTH) response, mice were immunized subcutaneously 2 and 4 weeks after oral OVA with 100 μg OVA in incomplete Freund's Adjuvant (Sigma #F5506). 3 weeks after the last immunization, mice were challenged with injection of 20 μg OVA (Sigma #A2512) into the footpad. Footpad thickness was measured blinded with micrometer calipers before footpad challenge and 24 hours after. For colon cytokine analysis, whole colons were washed in PBS and homogenized at 300 mg/ml in PBS plus protease inhibitor (Thermo Fisher #A32953). The homogenates were centrifuged repeatedly and supernatants isolated until no pellets were

visible. Supernatants were analyzed at 1:4 dilutions using the Bio-Plex Mouse Cytokine 23-plex Assay (BioRad #M60009RDPD) on the BioRad Bio-PlexTM 200 System with Bio-Plex Manager software. Limits of detection were defined using the standard curves' lowest concentrations of detectable cytokines. Cytokines that had values out of range for >2 samples were excluded from analysis. For *C. rodentium* infection, mice were infected with 5×10^7 CFU *C. rodentium* by gavage. *C. rodentium* CFUs were calculated by resuspending terminal pellets at 50 mg/ml in sterile PBS and after 24 hours of growth of serial dilutions on Macconkey at 37°C. For DSS + anti-IL10R treatment, mice were injected IP with anti-IL10R blocking antibody (BioXCell BE0050) and put on sterile 1% (w/v) DSS drinking water (TdB Labs 9011–18-1) before being switched to regular water after 1 week. For VAN antibiotic treatment, mice were put on control sterile drinking water or sterile drinking water containing 0.5 mg/ml vancomycin, 1 mg/ml ampicillin, and 1 mg/ml neomycin for one week.

QUANTIFICATION AND STATISTICAL ANALYSIS

Graphpad Prism v9 was used for used for statistical and graphical analysis unless noted. For *in vivo* experiments, each dot represents data from an individual host. In figures representing experiment means, n noted in the figure legend. Independent experimental replicates are indicated in the figure legends. Statistical tests utilized for individual experiments are noted in the figure legends. FDR, Sidak's or Dunnet's correction for multiple comparisons are used where noted. Significance was defined by $*p< 0.05$, $**p< 0.01$, ***p<0.001, ***p<0.0001.

Supplementary Material

Refer to Web version on PubMed Central for supplementary material.

Acknowledgements:

We would like to thank Nicole Santacruz and Patricia Hsieh for technical assistance (Wash.U.). C.-S.H. is supported by the grants U01 AI131349, R01 AI136515, R01 AI079187, BWF, and the Wolff Professorship. L.D.S. is supported by NIAID AI145496. E.R.G. is supported by NIH grants F30 DK111071 and T32 GM007200-42. Additional acknowledgements are provided in the supplement.

References

Aguirre SA, Mason PH, and Perryman LE (1994). Susceptibility of major histocompatibility complex (MHC) class I- and MHC class II-deficient mice to Cryptosporidium parvum infection. Infect Immun 62, 697–699. [PubMed: 7905464]

Ajuebor MN, Hogaboam CM, Kunkel SL, Proudfoot AE, and Wallace JL (2001). The chemokine RANTES is a crucial mediator of the progression from acute to chronic colitis in the rat. J Immunol 166, 552–558. [PubMed: 11123336]

Ansaldo E, Slayden LC, Ching KL, Koch MA, Wolf NK, Plichta DR, Brown EM, Graham DB, Xavier RJ, Moon JJ, and Barton GM (2019). Akkermansia muciniphila induces intestinal adaptive immune responses during homeostasis. Science 364, 1179–1184. [PubMed: 31221858]

Arpaia N, Campbell C, Fan X, Dikiy S, van der Veeken J, Deroos P, Liu H, Cross JR, Pfeffer K, Coffer PJ, and Rudensky AY (2013). Metabolites produced by commensal bacteria promote peripheral regulatory T-cell generation. Nature.

Barbosa JM, Costa-de-Oliveira S, Rodrigues AG, Hanscheid T, Shapiro H, and Pina-Vaz C (2008). A flow cytometric protocol for detection of Cryptosporidium spp. Cytometry A 73, 44–47. [PubMed: 18067124]

Barton ES, White DW, Cathelyn JS, Brett-McClellan KA, Engle M, Diamond MS, Miller VL, and Virgin H.W.t. (2007). Herpesvirus latency confers symbiotic protection from bacterial infection. Nature 447, 326–329. [PubMed: 17507983]

Berube J, Bourdon C, Yao Y, and Rousseau S (2009). Distinct intracellular signaling pathways control the synthesis of IL-8 and RANTES in TLR1/TLR2, TLR3 or NOD1 activated human airway epithelial cells. Cell Signal 21, 448–456. [PubMed: 19121387]

Bouziat R, Hinterleitner R, Brown JJ, Stencel-Baerenwald JE, Ikizler M, Mayassi T, Meisel M, Kim SM, Discepolo V, Pruijssers AJ, et al. (2017). Reovirus infection triggers inflammatory responses to dietary antigens and development of celiac disease. Science 356, 44–50. [PubMed: 28386004]

Bry L, Brigl M, and Brenner MB (2006). CD4+-T-cell effector functions and costimulatory requirements essential for surviving mucosal infection with Citrobacter rodentium. Infect Immun 74, 673–681. [PubMed: 16369024]

Callahan BJ, McMurdie PJ, Rosen MJ, Han AW, Johnson AJ, and Holmes SP (2016). DADA2: High-resolution sample inference from Illumina amplicon data. Nature methods 13, 581–583. [PubMed: 27214047]

Cama VA, Bern C, Roberts J, Cabrera L, Sterling CR, Ortega Y, Gilman RH, and Xiao L (2008). Cryptosporidium species and subtypes and clinical manifestations in children, Peru. Emerg Infect Dis 14, 1567–1574. [PubMed: 18826821]

Caporaso JG, Lauber CL, Walters WA, Berg-Lyons D, Lozupone CA, Turnbaugh PJ, Fierer N, and Knight R (2011). Global patterns of 16S rRNA diversity at a depth of millions of sequences per sample. Proceedings of the National Academy of Sciences of the United States of America 108 Suppl 1, 4516–4522. [PubMed: 20534432]

Chai JN, Peng Y, Rengarajan S, Solomon BD, Ai TL, Shen Z, Perry JSA, Knoop KA, Tanoue T, Narushima S, et al. (2017). Helicobacter species are potent drivers of colonic T cell responses in homeostasis and inflammation. Sci Immunol 2.

Charania R, Wade BE, McNair NN, and Mead JR (2020). Changes in the Microbiome of Cryptosporidium-Infected Mice Correlate to Differences in Susceptibility and Infection Levels. Microorganisms 8.

Checkley W, White AC Jr., Jaganath D, Arrowood MJ, Chalmers RM, Chen XM, Fayer R, Griffiths JK, Guerrant RL, Hedstrom L, et al. (2015). A review of the global burden, novel diagnostics, therapeutics, and vaccine targets for cryptosporidium. Lancet Infect Dis 15, 85–94. [PubMed: 25278220]

Chen W, Harp JA, and Harmsen AG (1993a). Requirements for CD4+ cells and gamma interferon in resolution of established Cryptosporidium parvum infection in mice. Infect Immun 61, 3928–3932. [PubMed: 8103040]

Chen W, Harp JA, Harmsen AG, and Havell EA (1993b). Gamma interferon functions in resistance to Cryptosporidium parvum infection in severe combined immunodeficient mice. Infect Immun 61, 3548–3551. [PubMed: 8335387]

Chudnovskiy A, Mortha A, Kana V, Kennard A, Ramirez JD, Rahman A, Remark R, Mogno I, Ng R, Gnjatic S, et al. (2016). Host-Protozoan Interactions Protect from Mucosal Infections through Activation of the Inflammasome. Cell 167, 444–456 e414. [PubMed: 27716507]

Collaborators, G.B.D.D.D. (2017). Estimates of global, regional, and national morbidity, mortality, and aetiologies of diarrhoeal diseases: a systematic analysis for the Global Burden of Disease Study 2015. Lancet Infect Dis 17, 909–948. [PubMed: 28579426]

Condlova S, Horcickova M, Havrdova N, Sak B, Hlaskova L, Perec-Matysiak A, Kicia M, McEvoy J, and Kvac M (2019). Diversity of Cryptosporidium spp. in Apodemus spp. in Europe. Eur J Protistol 69, 1–13. [PubMed: 30826667]

Cooper AM, and Khader SA (2007). IL-12p40: an inherently agonistic cytokine. Trends in immunology 28, 33–38. [PubMed: 17126601]

Cortez VS, and Colonna M (2016). Diversity and function of group 1 innate lymphoid cells. Immunology letters 179, 19–24. [PubMed: 27394699]

Current WL, and Reese NC (1986). A comparison of endogenous development of three isolates of Cryptosporidium in suckling mice. J Protozool 33, 98–108. [PubMed: 3959014]

Current WL, Reese NC, Ernst JV, Bailey WS, Heyman MB, and Weinstein WM (1983). Human cryptosporidiosis in immunocompetent and immunodeficient persons. Studies of an outbreak and experimental transmission. The New England journal of medicine 308, 1252–1257. [PubMed: 6843609]

Durai V, Bagadia P, Granja JM, Satpathy AT, Kulkarni DH, Davidson J.T.t., Wu R, Patel SJ, Iwata A, Liu TT, et al. (2019). Cryptic activation of an Irf8 enhancer governs cDC1 fate specification. Nat Immunol 20, 1161–1173. [PubMed: 31406378]

Elinav E, Strowig T, Kau AL, Henao-Mejia J, Thaiss CA, Booth CJ, Peaper DR, Bertin J, Eisenbarth SC, Gordon JI, and Flavell RA (2011). NLRP6 inflammasome regulates colonic microbial ecology and risk for colitis. Cell 145, 745–757. [PubMed: 21565393]

Escalante NK, Lemire P, Cruz Tleugabulova M, Prescott D, Mortha A, Streutker CJ, Girardin SE, Philpott DJ, and Mallevaey T (2016). The common mouse protozoa Tritrichomonas muris alters mucosal T cell homeostasis and colitis susceptibility. J Exp Med 213, 2841–2850. [PubMed: 27836928]

Esterhazy D, Canesso MCC, Mesin L, Muller PA, de Castro TBR, Lockhart A, ElJalby M, Faria AMC, and Mucida D (2019). Compartmentalized gut lymph node drainage dictates adaptive immune responses. Nature 569, 126–130. [PubMed: 30988509]

Farin HF, Karthaus WR, Kujala P, Rakhshandehroo M, Schwank G, Vries RG, Kalkhoven E, Nieuwenhuis EE, and Clevers H (2014). Paneth cell extrusion and release of antimicrobial products is directly controlled by immune cell-derived IFN-gamma. J Exp Med 211, 1393–1405. [PubMed: 24980747]

Fayer R, Santin M, and Macarisin D (2010). Cryptosporidium ubiquitum n. sp. in animals and humans. Vet Parasitol 172, 23–32. [PubMed: 20537798]

Flanigan TP, and Soave R (1993). Cryptosporidiosis. Prog Clin Parasitol 3, 1–20. [PubMed: 8420600]

Furusawa Y, Obata Y, Fukuda S, Endo TA, Nakato G, Takahashi D, Nakanishi Y, Uetake C, Kato K, Kato T, et al. (2013). Commensal microbe-derived butyrate induces the differentiation of colonic regulatory T cells. Nature.

Gharpure R, Perez A, Miller AD, Wikswo ME, Silver R, and Hlavsa MC (2019). Cryptosporidiosis Outbreaks - United States, 2009–2017. MMWR Morb Mortal Wkly Rep 68, 568–572. [PubMed: 31246941]

Groom JR (2019). Regulators of T-cell fate: Integration of cell migration, differentiation and function. Immunol Rev 289, 101–114. [PubMed: 30977199]

Gupta J, and Nebreda AR (2014). Analysis of Intestinal Permeability in Mice. Bio-protocol 4, e1289.

Hand TW, Dos Santos LM, Bouladoux N, Molloy MJ, Pagan AJ, Pepper M, Maynard CL, Elson CO 3rd, and Belkaid Y (2012). Acute gastrointestinal infection induces long-lived microbiota-specific T cell responses. Science 337, 1553–1556. [PubMed: 22923434]

Heine J, Moon HW, and Woodmansee DB (1984). Persistent Cryptosporidium infection in congenitally athymic (nude) mice. Infect Immun 43, 856–859. [PubMed: 6607888]

Hildner K, Edelson BT, Purtha WE, Diamond M, Matsushita H, Kohyama M, Calderon B, Schraml BU, Unanue ER, Diamond MS, et al. (2008). Batf3 deficiency reveals a critical role for CD8alpha+ dendritic cells in cytotoxic T cell immunity. Science 322, 1097–1100. [PubMed: 19008445]

Hsieh C-S, Liang Y, Tyznik AJ, Self SG, Liggitt D, and Rudensky AY (2004). Recognition of the peripheral self by naturally arising CD25+ CD4+ T cell receptors. Immunity 21, 267–277. [PubMed: 15308106]

Hsieh CS, Macatonia SE, Tripp CS, Wolf SF, O'Garra A, and Murphy KM (1993). Development of TH1 CD4+ T cells through IL-12 produced by Listeria-induced macrophages. Science 260, 547–549. [PubMed: 8097338]

Huang J, Mullapudi N, Lancto CA, Scott M, Abrahamsen MS, and Kissinger JC (2004). Phylogenomic evidence supports past endosymbiosis, intracellular and horizontal gene transfer in Cryptosporidium parvum. Genome Biol 5, R88. [PubMed: 15535864]

Ise W, Kohyama M, Nutsch KM, Lee HM, Suri A, Unanue ER, Murphy TL, and Murphy KM (2010). CTLA-4 suppresses the pathogenicity of self antigen-specific T cells by cell-intrinsic and cell-extrinsic mechanisms. Nat Immunol 11, 129–135. [PubMed: 20037585]

Ivanov II, Atarashi K, Manel N, Brodie EL, Shima T, Karaoz U, Wei D, Goldfarb KC, Santee CA, Lynch SV, et al. (2009). Induction of intestinal Th17 cells by segmented filamentous bacteria. Cell 139, 485–498. [PubMed: 19836068]

Iwano S, Sugiyama M, Hama H, Watakabe A, Hasegawa N, Kuchimaru T, Tanaka KZ, Takahashi M, Ishida Y, Hata J, et al. (2018). Single-cell bioluminescence imaging of deep tissue in freely moving animals. Science 359, 935–939. [PubMed: 29472486]

Jankovic D, Kullberg MC, Feng CG, Goldszmid RS, Collazo CM, Wilson M, Wynn TA, Kamanaka M, Flavell RA, and Sher A (2007). Conventional T-bet(+)Foxp3(−) Th1 cells are the major source of host-protective regulatory IL-10 during intracellular protozoan infection. J Exp Med 204, 273–283. [PubMed: 17283209]

Kaplan DH, Jenison MC, Saeland S, Shlomchik WD, and Shlomchik MJ (2005). Epidermal langerhans cell-deficient mice develop enhanced contact hypersensitivity. Immunity 23, 611–620. [PubMed: 16356859]

Kominsky DJ, Campbell EL, Ehrentraut SF, Wilson KE, Kelly CJ, Glover LE, Collins CB, Bayless AJ, Saeedi B, Dobrinskikh E, et al. (2014). IFN-gamma-mediated induction of an apical IL-10 receptor on polarized intestinal epithelia. J Immunol 192, 1267–1276. [PubMed: 24367025]

Kotloff KL, Nasrin D, Blackwelder WC, Wu Y, Farag T, Panchalingham S, Sow SO, Sur D, Zaidi AKM, Faruque ASG, et al. (2019). The incidence, aetiology, and adverse clinical consequences of less severe diarrhoeal episodes among infants and children residing in low-income and middle-income countries: a 12-month case-control study as a follow-on to the Global Enteric Multicenter Study (GEMS). Lancet Glob Health 7, e568–e584. [PubMed: 31000128]

Kuhls TL, Greenfield RA, Mosier DA, Crawford DL, and Joyce WA (1992). Cryptosporidiosis in adult and neonatal mice with severe combined immunodeficiency. J Comp Pathol 106, 399–410. [PubMed: 1644934]

Kulkarni DH, Gustafsson JK, Knoop KA, McDonald KG, Bidani SS, Davis JE, Floyd AN, Hogan SP, Hsieh CS, and Newberry RD (2020). Goblet cell associated antigen passages support the induction and maintenance of oral tolerance. Mucosal Immunol 13, 271–282. [PubMed: 31819172]

Lathrop SK, Bloom SM, Rao SM, Nutsch K, Lio CW, Santacruz N, Peterson DA, Stappenbeck TS, and Hsieh CS (2011). Peripheral education of the immune system by colonic commensal microbiota. Nature 478, 250–254. [PubMed: 21937990]

Leitch GJ, and He Q (2012). Cryptosporidiosis-an overview. J Biomed Res 25, 1–16. [PubMed: 22685452]

Liu J, Guan X, and Ma X (2005). Interferon regulatory factor 1 is an essential and direct transcriptional activator for interferon {gamma}-induced RANTES/CCl5 expression in macrophages. The Journal of biological chemistry 280, 24347–24355. [PubMed: 15860458]

Lv C, Zhang L, Wang R, Jian F, Zhang S, Ning C, Wang H, Feng C, Wang X, Ren X, et al. (2009). Cryptosporidium spp. in wild, laboratory, and pet rodents in china: prevalence and molecular characterization. Appl Environ Microbiol 75, 7692–7699. [PubMed: 19820152]

Mashayekhi M, Sandau MM, Dunay IR, Frickel EM, Khan A, Goldszmid RS, Sher A, Ploegh HL, Murphy TL, Sibley LD, and Murphy KM (2011). CD8alpha(+) dendritic cells are the critical source of interleukin-12 that controls acute infection by Toxoplasma gondii tachyzoites. Immunity 35, 249–259. [PubMed: 21867928]

McDonald V, Robinson HA, Kelly JP, and Bancroft GJ (1994). Cryptosporidium muris in adult mice: adoptive transfer of immunity and protective roles of CD4 versus CD8 cells. Infect Immun 62, 2289–2294. [PubMed: 7910592]

Mead JR, Arrowood MJ, Sidwell RW, and Healey MC (1991). Chronic Cryptosporidium parvum infections in congenitally immunodeficient SCID and nude mice. J Infect Dis 163, 1297–1304. [PubMed: 2037795]

Mondal D, Minak J, Alam M, Liu Y, Dai J, Korpe P, Liu L, Haque R, and Petri WA Jr. (2012). Contribution of enteric infection, altered intestinal barrier function, and maternal malnutrition to infant malnutrition in Bangladesh. Clin Infect Dis 54, 185–192. [PubMed: 22109945]

Morgan-Ryan UM, Fall A, Ward LA, Hijjawi N, Sulaiman I, Fayer R, Thompson RC, Olson M, Lal A, and Xiao L (2002). Cryptosporidium hominis n. sp. (Apicomplexa: Cryptosporidiidae) from Homo sapiens. J Eukaryot Microbiol 49, 433–440. [PubMed: 12503676]

Morgan UM, Sturdee AP, Singleton G, Gomez MS, Gracenea M, Torres J, Hamilton SG, Woodside DP, and Thompson RC (1999). The Cryptosporidium “mouse” genotype is conserved across geographic areas. J Clin Microbiol 37, 1302–1305. [PubMed: 10203475]

Nava P, Koch S, Laukoetter MG, Lee WY, Kolegraff K, Capaldo CT, Beeman N, Addis C, Gerner-Smidt K, Neumaier I, et al. (2010). Interferon-gamma regulates intestinal epithelial homeostasis through converging beta-catenin signaling pathways. Immunity 32, 392–402. [PubMed: 20303298]

Nutsch K, Chai JN, Ai TL, Russler-Germain E, Feehley T, Nagler CR, and Hsieh CS (2016). Rapid and Efficient Generation of Regulatory T Cells to Commensal Antigens in the Periphery. Cell Rep 17, 206–220. [PubMed: 27681432]

Osman M, Benamrouz S, Guyot K, Baydoun M, Frealle E, Chabe M, Gantois N, Delaire B, Goffard A, Aoun A, et al. (2017a). High association of Cryptosporidium spp. infection with colon adenocarcinoma in Lebanese patients. PLoS One 12, e0189422. [PubMed: 29261714]

Osman M, El Safadi D, Benamrouz-Vanneste S, Cian A, Moriniere R, Gantois N, Delgado-Viscogliosi P, Guyot K, Bosc S, Chabe M, et al. (2017b). Prevalence, transmission, and host specificity of Cryptosporidium spp. in various animal groups from two French zoos. Parasitol Res 116, 3419–3422. [PubMed: 29030716]

Petersen C (1992). Cryptosporidiosis in patients infected with the human immunodeficiency virus. Clin Infect Dis 15, 903–909. [PubMed: 1457661]

Pollok RC, Farthing MJ, Bajaj-Elliott M, Sanderson IR, and McDonald V (2001). Interferon gamma induces enterocyte resistance against infection by the intracellular pathogen Cryptosporidium parvum. Gastroenterology 120, 99–107. [PubMed: 11208718]

Potiron L, Lacroix-Lamande S, Marquis M, Levern Y, Fort G, Franceschini I, and Laurent F (2019). Batf3-Dependent Intestinal Dendritic Cells Play a Critical Role in the Control of Cryptosporidium parvum Infection. J Infect Dis 219, 925–935. [PubMed: 30203075]

Reinhardt RL, Liang HE, and Locksley RM (2009). Cytokine-secreting follicular T cells shape the antibody repertoire. Nat Immunol 10, 385–393. [PubMed: 19252490]

Ren X, Zhao J, Zhang L, Ning C, Jian F, Wang R, Lv C, Wang Q, Arrowood MJ, and Xiao L (2012). Cryptosporidium tyzzeri n. sp. (Apicomplexa: Cryptosporidiidae) in domestic mice (Mus musculus). Exp Parasitol 130, 274–281. [PubMed: 21803038]

Roncarolo MG, Gregori S, Bacchetta R, Battaglia M, and Gagliani N (2018). The Biology of T Regulatory Type 1 Cells and Their Therapeutic Application in Immune-Mediated Diseases. Immunity 49, 1004–1019. [PubMed: 30566879]

Sadick MD, Heinzel FP, Holaday BJ, Pu RT, Dawkins RS, and Locksley RM (1990). Cure of murine leishmaniasis with anti-interleukin 4 monoclonal antibody. Evidence for a T cell-dependent, interferon gamma-independent mechanism. J Exp Med 171, 115–127. [PubMed: 2104918]

Sateriale A, Slapeta J, Baptista R, Engiles JB, Gullicksrud JA, Herbert GT, Brooks CF, Kugler EM, Kissinger JC, Hunter CA, and Striepen B (2019). A Genetically Tractable, Natural Mouse Model of Cryptosporidiosis Offers Insights into Host Protective Immunity. Cell Host Microbe 26, 135–146 e135. [PubMed: 31231045]

Scallan E, Hoekstra RM, Angulo FJ, Tauxe RV, Widdowson MA, Roy SL, Jones JL, and Griffin PM (2011). Foodborne illness acquired in the United States--major pathogens. Emerg Infect Dis 17, 7–15. [PubMed: 21192848]

Schall TJ, Bacon K, Toy KJ, and Goeddel DV (1990). Selective attraction of monocytes and T lymphocytes of the memory phenotype by cytokine RANTES. Nature 347, 669–671. [PubMed: 1699135]

Schoenborn JR, and Wilson CB (2007). Regulation of interferon-gamma during innate and adaptive immune responses. Adv Immunol 96, 41–101. [PubMed: 17981204]

Scott P, Natovitz P, Coffman RL, Pearce E, and Sher A (1988). Immunoregulation of cutaneous leishmaniasis. T cell lines that transfer protective immunity or exacerbation belong to different T helper subsets and respond to distinct parasite antigens. J Exp Med 168, 1675–1684. [PubMed: 2903212]

Shiomi H, Masuda A, Nishiumi S, Nishida M, Takagawa T, Shiomi Y, Kutsumi H, Blumberg RS, Azuma T, and Yoshida M (2010). Gamma interferon produced by antigen-specific CD4+ T cells regulates the mucosal immune responses to Citrobacter rodentium infection. Infect Immun 78, 2653–2666. [PubMed: 20351140]

Smith PM, Howitt MR, Panikov N, Michaud M, Gallini CA, Bohlooly YM, Glickman JN, and Garrett WS (2013). The microbial metabolites, short-chain fatty acids, regulate colonic Treg cell homeostasis. Science 341, 569–573. [PubMed: 23828891]

Solomon BD, and Hsieh CS (2016). Antigen-Specific Development of Mucosal Foxp3+RORγt+ T Cells from Regulatory T Cell Precursors. J Immunol 197, 3512–3519. [PubMed: 27671109]

Spahn TW, Ross M, von Eiff C, Maaser C, Spieker T, Kannengiesser K, Domschke W, and Kucharzik T (2008). CD4+ T cells transfer resistance against Citrobacter rodentium-induced infectious colitis by induction of Th 1 immunity. Scandinavian journal of immunology 67, 238–244. [PubMed: 18261038]

Stensvold CR, Beser J, Axen C, and Lebbad M (2014). High applicability of a novel method for gp60-based subtyping of Cryptosporidium meleagridis. J Clin Microbiol 52, 2311–2319. [PubMed: 24740082]

Sulzyc-Bielicka V, Kolodziejczyk L, Jaczewska S, Bielicki D, Safranow K, Bielicki P, Kladny J, and Rogowski W (2018). Colorectal cancer and Cryptosporidium spp. infection. PLoS One 13, e0195834. [PubMed: 29672572]

Tandel J, English ED, Sateriale A, Gullicksrud JA, Beiting DP, Sullivan MC, Pinkston B, and Striepen B (2019). Life cycle progression and sexual development of the apicomplexan parasite Cryptosporidium parvum. Nat Microbiol 4, 2226–2236. [PubMed: 31477896]

Terzic J, Grivennikov S, Karin E, and Karin M (2010). Inflammation and colon cancer. Gastroenterology 138, 2101–2114 e2105. [PubMed: 20420949]

Tessema TS, Schwamb B, Lochner M, Forster I, Jakobi V, and Petry F (2009). Dynamics of gut mucosal and systemic Th1/Th2 cytokine responses in interferon-gamma and interleukin-12p40 knock out mice during primary and challenge Cryptosporidium parvum infection. Immunobiology 214, 454–466. [PubMed: 19155092]

Theodos CM, Sullivan KL, Griffiths JK, and Tzipori S (1997). Profiles of healing and nonhealing Cryptosporidium parvum infection in C57BL/6 mice with functional B and T lymphocytes: the extent of gamma interferon modulation determines the outcome of infection. Infect Immun 65, 4761–4769. [PubMed: 9353062]

Tussiwand R, Lee WL, Murphy TL, Mashayekhi M, Kc W, Albring JC, Satpathy AT, Rotondo JA, Edelson BT, Kretzer NM, et al. (2012). Compensatory dendritic cell development mediated by BATF-IRF interactions. Nature 490, 502–507. [PubMed: 22992524]

Upton SJ, and Current WL (1985). The species of Cryptosporidium (Apicomplexa: Cryptosporidiidae) infecting mammals. J Parasitol 71, 625–629. [PubMed: 4057006]

Urban JF Jr., Fayer R, Chen SJ, Gause WC, Gately MK, and Finkelman FD (1996). IL-12 protects immunocompetent and immunodeficient neonatal mice against infection with Cryptosporidium parvum. J Immunol 156, 263–268. [PubMed: 8598471]

Vallance BA, Deng W, Jacobson K, and Finlay BB (2003). Host susceptibility to the attaching and effacing bacterial pathogen Citrobacter rodentium. Infect Immun 71, 3443–3453. [PubMed: 12761129]

Vaughan JA, Noden BH, and Beier JC (1991). Concentrations of human erythrocytes by anopheline mosquitoes (Diptera: Culicidae) during feeding. J Med Entomol 28, 780–786. [PubMed: 1770513]

Welty NE, Staley C, Ghilardi N, Sadowsky MJ, Igyarto BZ, and Kaplan DH (2013). Intestinal lamina propria dendritic cells maintain T cell homeostasis but do not affect commensalism. J Exp Med 210, 2011–2024. [PubMed: 24019552]

Wilke G, Funkhouser-Jones LJ, Wang Y, Ravindran S, Wang Q, Beatty WL, Baldridge MT, VanDussen KL, Shen B, Kuhlenschmidt MS, et al. (2019). A Stem-Cell-Derived Platform Enables Complete Cryptosporidium Development In Vitro and Genetic Tractability. Cell Host Microbe 26, 123–134 e128. [PubMed: 31231046]

Wilke G, Ravindran S, Funkhouser-Jones L, Barks J, Wang Q, VanDussen KL, Stappenbeck TS, Kuhlenschmidt TB, Kuhlenschmidt MS, and Sibley LD (2018). Monoclonal Antibodies to

Intracellular Stages of Cryptosporidium parvum Define Life Cycle Progression In Vitro. mSphere 3.

Wong P, Goldrath AW, and Rudensky AY (2000). Competition for specific intrathymic ligands limits positive selection in a TCR transgenic model of CD4+ T cell development. J Immunol 164, 6252–6259. [PubMed: 10843678]

Xiao L (2010). Molecular epidemiology of cryptosporidiosis: an update. Exp Parasitol 124, 80–89. [PubMed: 19358845]

Xu M, Pokrovskii M, Ding Y, Yi R, Au C, Harrison OJ, Galan C, Belkaid Y, Bonneau R, and Littman DR (2018). c-MAF-dependent regulatory T cells mediate immunological tolerance to a gut pathobiont. Nature 554, 373–377. [PubMed: 29414937]

Highlights

- *Cryptosporidium tyzzeri* in our colony (*Ct*-STL) is a commensal pathobiont
- *Ct*-STL elicits a dominant antigen-specific Th1 response
- cDC1s are required for efficient Th1 induction and blockade of Th17/Treg generation
- *Ct*-STL markedly impacts the immune system of both the small and large intestine

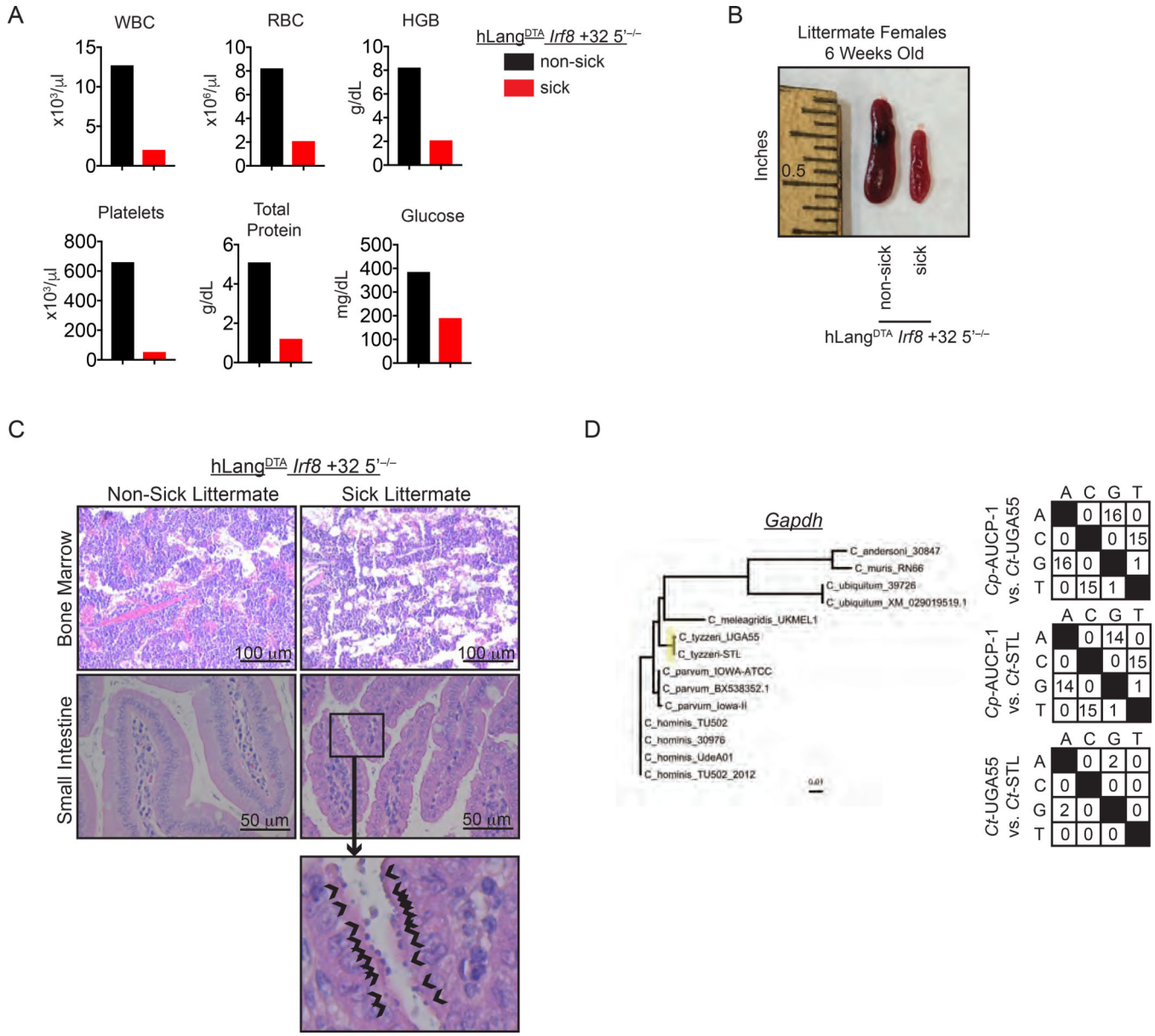

Figure 1. cDC1-deficient mice develop fulminant cryptosporidiosis

(A) Complete blood cell counts, total protein, and glucose from peripheral blood of a spontaneously sick 7-week-old cDC1-deficient mouse (hLang^{DTA} *Irf8* +32 5'$^{-/-}$) compared with a non-sick littermate (*Irf8* +32 5'$^{-/-}$). (B) Spleen size of a spontaneously sick 6-week-old cDC1-deficient mouse (hLang^{DTA} *Irf8* +32 5'$^{-/-}$) compared with a non-sick littermate. (C) Bone marrow and SI histology from mice in (A). Arrowheads indicate *Cryptosporidium* parasites in the SI epithelium. (D) Alignment and clustering of *Ct*-STL *Gapdh* sequence with *Gapdh* sequences from other *Cryptosporidium* species (left). The number of nucleotide differences in *Gapdh* between *Cp*-AUCP-1, *Ct*-UGA55, and *Ct*-STL are shown (right).

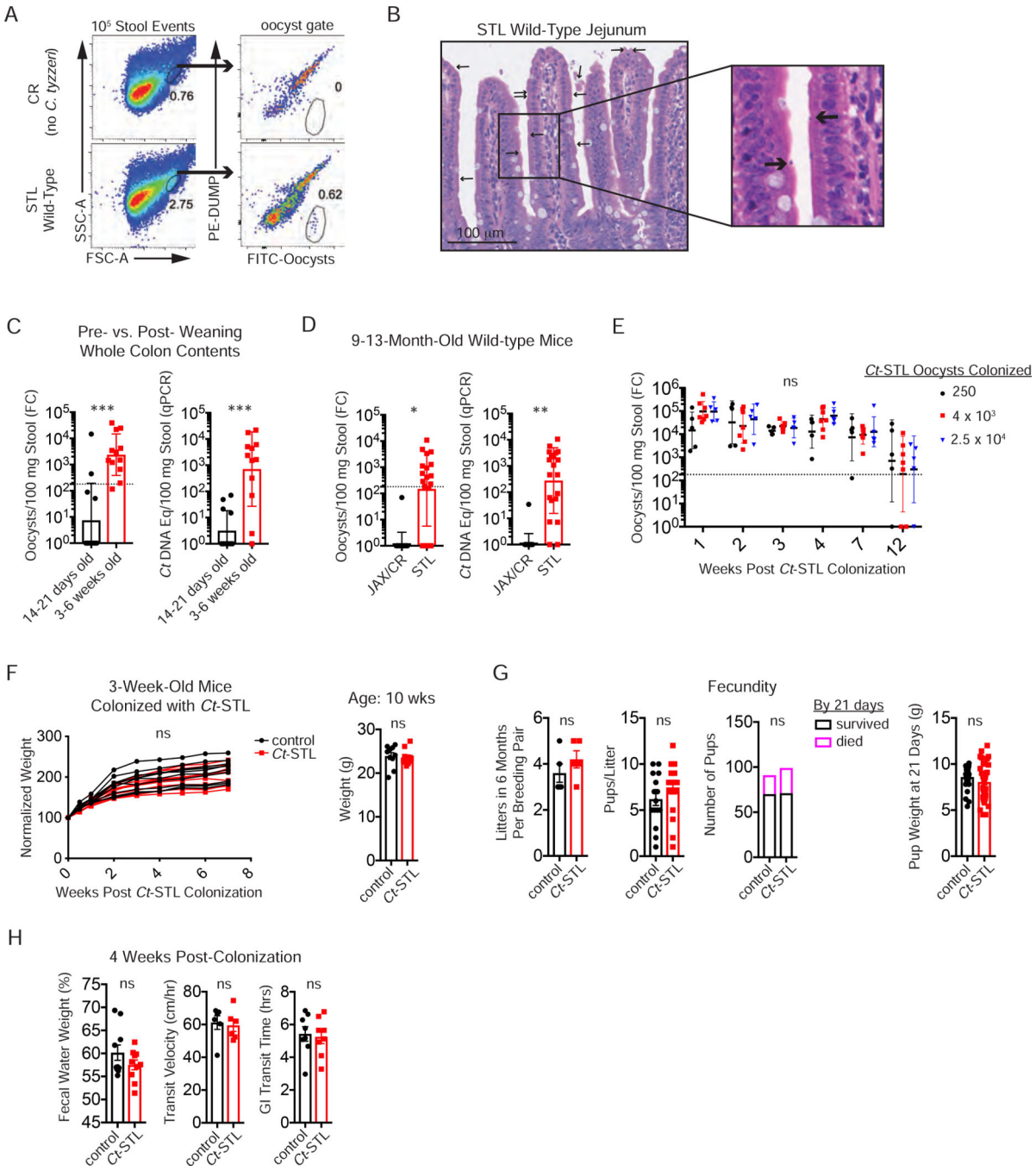

Figure 2. *Ct*-STL behaves like a commensal in WT mice

(A) Quantification of *Ct*-STL oocysts in terminal pellets by flow cytometry (FC) using Crypto-a-Glo of a *Cryptosporidium*-free Charles River (CR) vs a WT mouse from our colony (STL Wild-Type). 10^5 total events are displayed on the left; oocysts in the gate represent total oocysts in 10^5 stool events. (B) *Ct*-STL parasites within the jejunum brush border (arrows) in STL WT mice by histology. (C) *Ct*-STL quantification by FC and qPCR of stool DNA in whole luminal colon contents from STL WT mice before and after weaning (14–21 days and 3–6 weeks old, respectively). FC and qPCR samples were

from different mice. Dotted line in FC represents the limit of specific detection determined using *Cryptosporidium*-free mice (expt.=2). (D) *Ct*-STL quantification by FC and qPCR in the terminal pellets of 9–13 month old mice with JAX or CR microbiota versus similarly-aged STL WT mice. FC and qPCR samples were from identical mice (expt.=2). (E) FC quantification of *Ct*-STL in terminal pellets of WT CR mice colonized at 3.5 weeks of age with 250, 4×10^3, or 2.5×10^4 *Ct*-STL oocysts (expt.=3). (F) Normalized (left) and absolute (right) weights of CR mice colonized with 4×10^3 *Ct*-STL oocysts at 3.5 weeks of age (expt.=2). (G) Fecundity of *Ct*-STL colonized mice. Littermate CR mice were gavaged with 4×10^3 *Ct*-STL oocysts or PBS (control) at 3.5 weeks of age and set up as breeding pairs at 6 weeks of age. Number of litters per breeding pair (far left), pups born per litter (mid left), number of pups dead or alive at 21 days of life (mid right), and pup weights at 21 days (far right) were quantified over 6 months (expt.=5). (H) Fecal water weight of terminal pellets (left), transit velocity of gavaged dye (mid), and total gastrointestinal (GI) transit time (right) in *Ct*-STL colonized vs. control CR mice. WT CR mice were gavaged with 4×10^3 *Ct*-STL oocysts or PBS (control) at 3.5 weeks old and mice were assessed after 4 weeks (expt.=2). Each dot represents data from an individual host. Geometric mean ± geometric S.D. (C–E) or mean ± S.E.M. (F right, G, H) are shown. Student's t-test (C, D, F right, G, H), repeated measures ANOVA (E, F left), or Fisher's exact test (G mid right) p-values are shown.

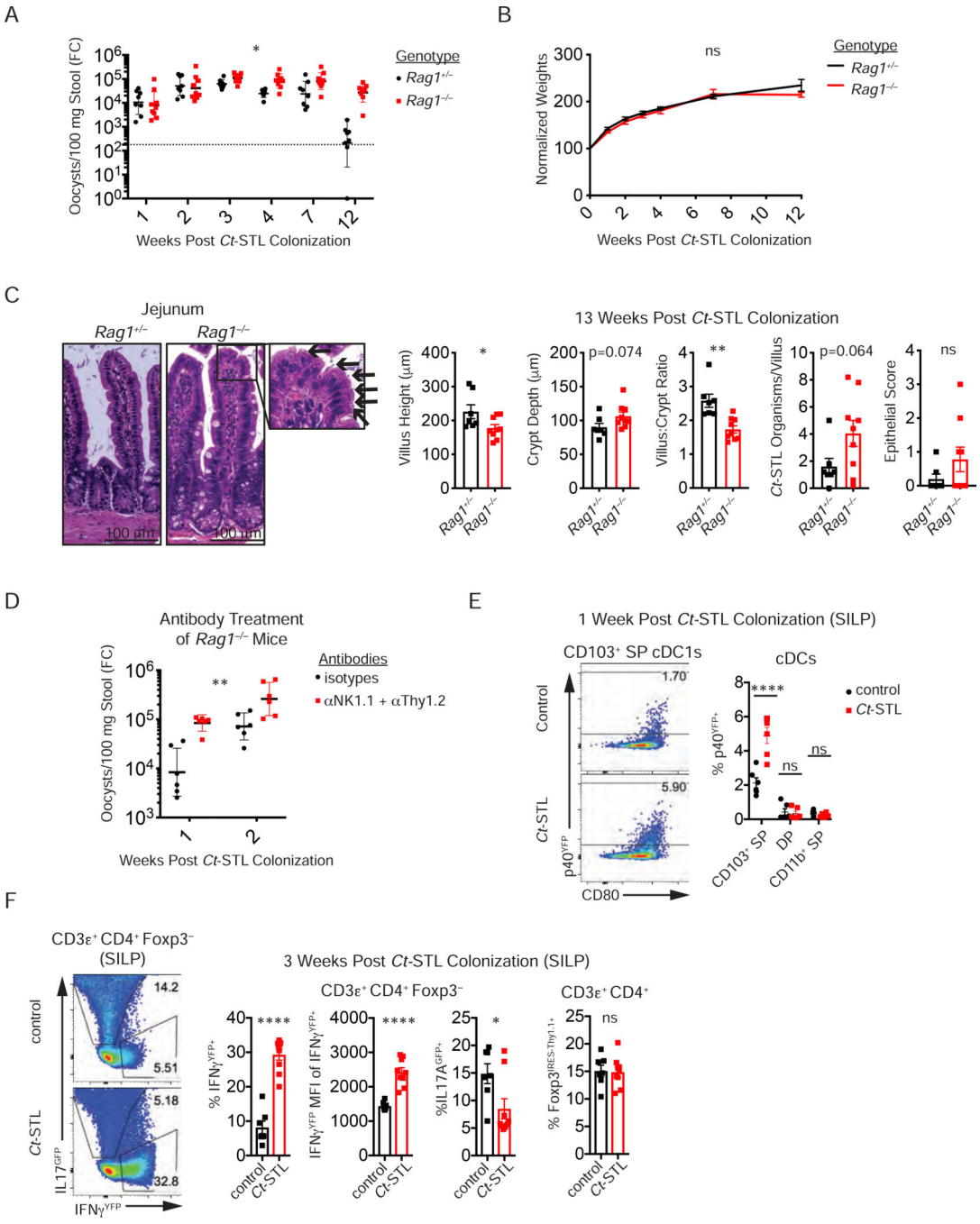

Figure 3. Both innate and adaptive immunity are required to limit *Ct*-STL

(A-C) *Ct*-STL oocyst shedding in terminal pellets by FC (A), weight loss (B), and jejunum histology at 13 weeks (C, arrows indicate *Ct*-STL parasites) in littermate *Rag1*$^{+/-}$ and *Rag1*$^{-/-}$ mice after colonization with 4×10^3 *Ct*-STL oocysts at 3 weeks of age (expt.=2). Weights were normalized to starting weights. (D) Quantification of *Ct*-STL oocysts by FC after depletion of innate immune cells with anti-NK1.1 and anti-Thy1.2 or isotype control treatment in *Rag1*$^{-/-}$ mice colonized with *Ct*-STL at weaning (expt=2). (E) IL-12p40^{YFP} expression in SILP cDC (MHCII$^+$ CD11c$^+$ F4/80$^-$) subsets 1 week after colonization

with *Ct*-STL. DP = double positive ($CD103^+$ $CD11b^+$), SP = single positive (expt.=2). (F) Expression of $IFN\gamma^{YFP}$ $IL17A^{GFP}$ $Foxp3^{IRES\text{-}Thy1.1}$ in SILP $CD4^+$ T cells 3 weeks after colonization with *Ct*-STL (expt.=3). Each dot represents data from an individual host. Geometric mean ± geometric S.D. (A, D) or mean ± S.E.M. (B, C, E, F) are shown. P-values from Student's t-test (C, F), ANOVA with Sidak's correction (E), repeated measures ANOVA (A, D), or repeated measures mixed effects analysis (B), are shown.

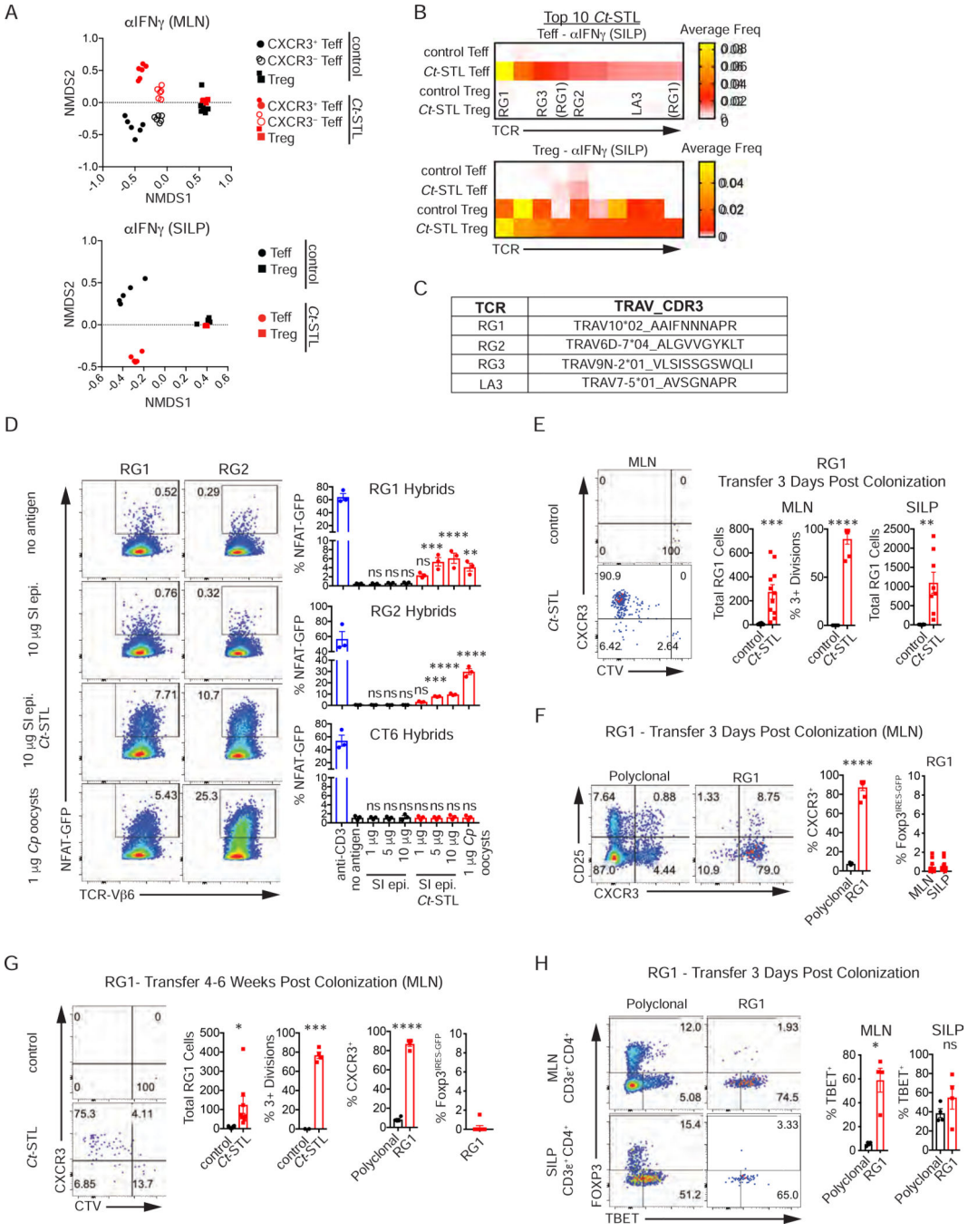

Figure 4. *Ct*-STL induces an antigen-specific Th1 response

(A-C) CD4$^+$ T cell TCR repertoire changes in anti-IFNγ-treated *Ct*-STL colonized mice. Fixed TCRβ *Foxp3*^{GFP} *Tcra*$^{+/-}$ mice were gavaged with 2.5–5×10^4 *Ct*-STL oocysts or PBS and treated weekly with anti-IFNγ to increase *Ct*-STL burden. TCRα chain sequencing was performed on CD4$^+$ Teff (CD62L^{lo} CD44^{hi} Foxp3$^-$) and Treg (Foxp3$^+$) populations after 2–3 weeks (expt.=3). (A) Bray-Curtis NMDS analysis of TCRα sequences from the MLN (top) or SILP (bottom). (B) Heatmaps representing the mean frequencies of the top 10 Teff (top) or Treg (bottom) TCRs in the SILP in *Ct*-STL colonized mice. TCRs selected

for functional studies are noted (RG1–3, LA3). RG1-like TCRs with TRAV differences are indicated by (RG1) (n=5 for each group). (C) TRAV and CDR3 amino acid sequences for *Ct*-STL specific TCRs are shown. (D) RG1 and RG2 TCR-transduced T cell hybridoma cells were cultured together with the indicated antigen presented by splenic Flt3L-induced $CD11c^+$ cells. Anti-CD3 was used as a positive control. NFAT-GFP expression was analyzed after 40 hours (expt.=3). (E-H) *In vivo* analysis of RG1 TCR. 2×10^4 (E-G) or 10^5 (H) retroviral RG1-expressing TCli-αβ $Foxp3^{IRES\text{-}GFP}$ T cells were transferred into *Ct*-STL colonized mice and analyzed 1 week later (expt.=2). (E) CTV-labeled RG1 T cell expansion in mice colonized with *Ct*-STL for 3 days. (F) RG1 T cell expression of CXCR3, CD25, and Foxp3 in *Ct*-STL colonized mice for 3 days. CXCR3 and CD25 on host polyclonal MLN $CD4^+$ T cells are also shown. (G) CTV-labeled RG1 T cell expansion and expression of CXCR3 and Foxp3 in mice colonized with *Ct*-STL for 4–6 weeks. (H) RG1 T cell expression of Tbet and FoxP3 transcription factor staining in mice colonized with *Ct*-STL for 3 days. Each dot represents data from an individual host (A, E-H) or mean of 2 *in vitro* co-cultures (D). Mean ± S.E.M. is shown. Student's t-test (E-H) or ANOVA with Dunnett's correction (D) p-values are shown.

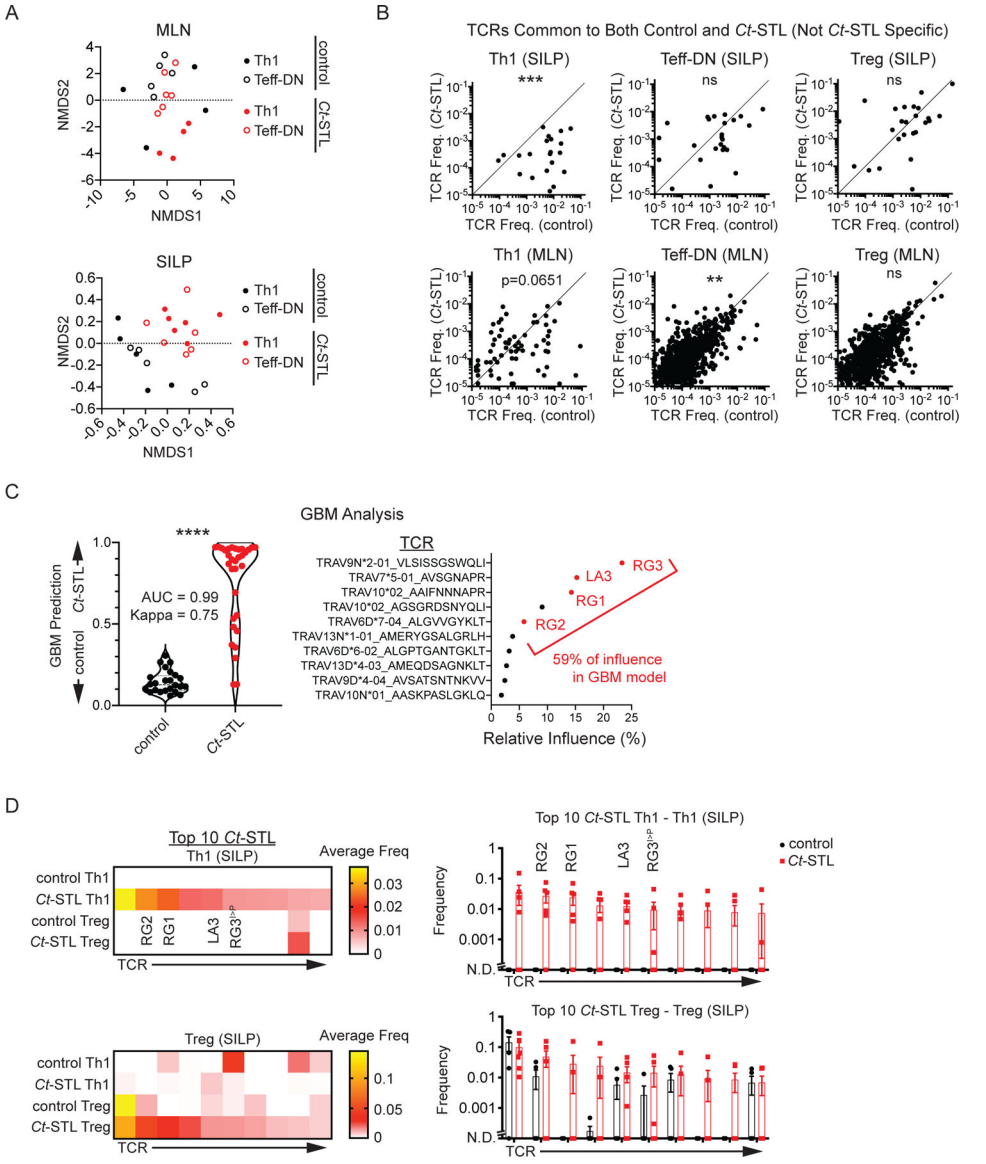

Figure 5. *Ct*-STL colonization alters the small intestine TCR repertoire at homeostasis

(A-D) CD4^{+} T cell TCR repertoire analysis of the SILP and MLN. Fixed TCRβ IFNγ^{YFP} IL17^{GFP} Foxp3$^{IRES\text{-}Thy1.1}$ *Tcra*$^{+/-}$ mice were colonized with *Ct*-STL at weaning for 3 weeks before sorting CD4^{+} CD62L^{lo} CD44^{hi} Th1 (Foxp3^{-} IFNγ^{YFP+} IL17^{GFP-}), Teff-DN (Foxp3^{-} IFNγ^{YFP-} IL17^{GFP-}) and Treg (Foxp3^{+}) populations (n=5–6, expt.=3 for SILP and MLN DN and Treg; n=4, expt.=2 for MLN Th1). (A) Bray-Curtis NMDS analysis of Teff TCRα sequences. Each dot indicates a T cell subset from an individual mouse. (B) Comparison of non-*Cryptosporidium* dependent TCR frequencies in control and *Ct*-STL colonized mice. Mean frequency of TCRs found in both control and *Ct*-STL data sets are plotted (see Methods). Each dot represents the mean frequency of an individual TCR that was found in at least 1 control mouse and at least one *Ct*-STL colonized mouse. (C) Identification of TCRs that distinguish between *Ct*-STL and control by machine learning. GBM was used to classify control vs *Ct*-STL using the data from Th1 and Teff-DN cells from the MLN, SILP,

and colon (see Methods). Data shown are the average prediction values for each sample (left) and the average relative influence for each TCR. (D) Analysis of SILP top 10 Th1 and Treg TCRs by heatmap (left, average frequency) and frequency bar plot (right). RG3-like TCR with CDR3 amino acid difference is indicated by superscript. Each dot represents data from an individual host (A, D right) or individual TCR (B-C). Violin plot with median and quartiles (C left) or mean ± S.E.M (D right) are shown. Paired t-test (B) and Mann-Whitney U (C left) p-values are shown. N.D. = not detected.

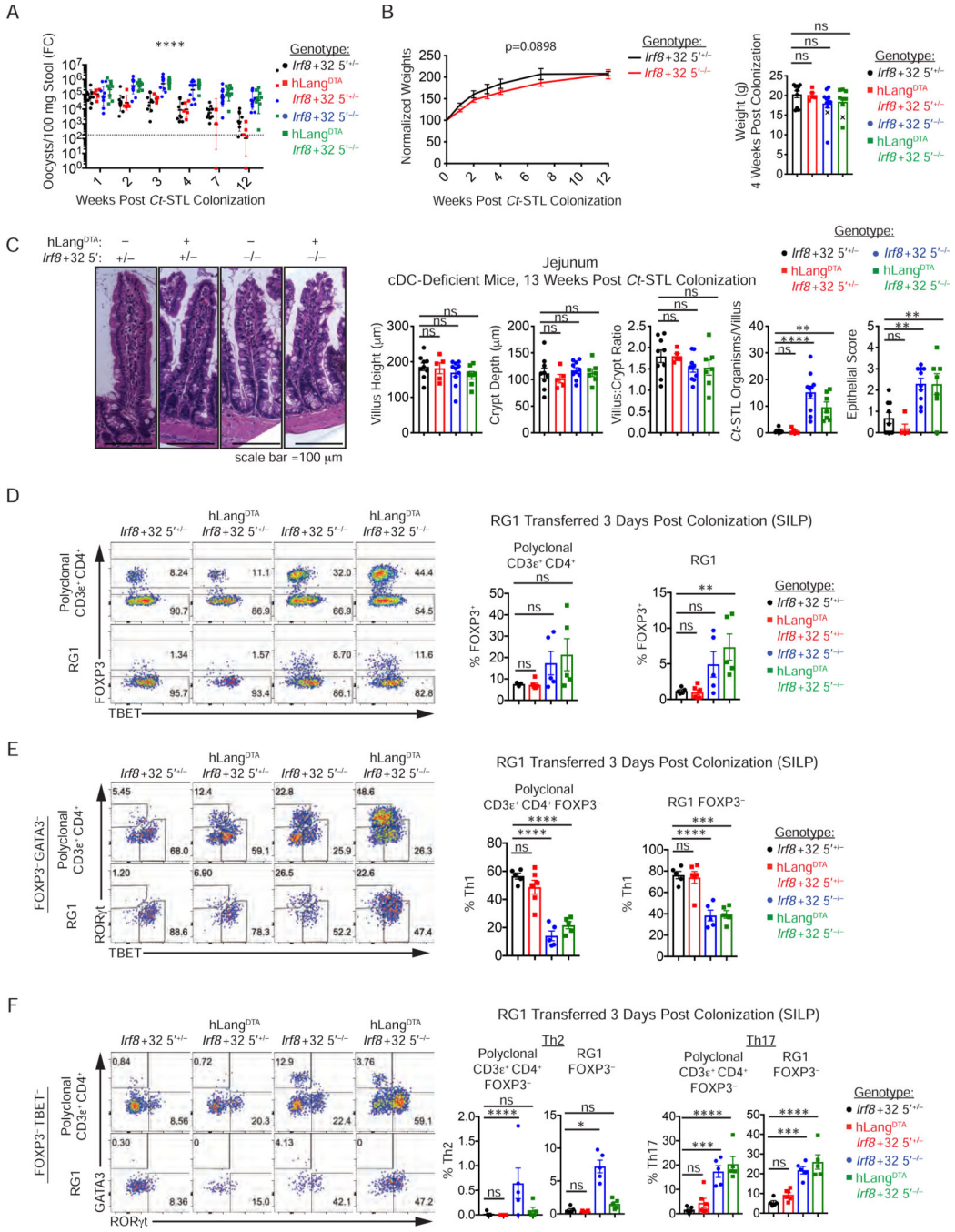

Figure 6. cDC1s are important for *Ct*-STL control and Th1 differentiation

(A-C) Littermate cDC subset-deficient hLang^{DTA} *Irf8* +32 5' mice were colonized at weaning with *Ct*-STL (expt.=4) and tracked for (A) oocyst shedding using flow cytometry, and (B) weight change. "X" symbols in (B, right) indicate mice that died between 7–12 weeks after *Ct*-STL colonization. (C) Histologic analysis of jejunums 13 weeks after *Ct*-STL colonization. (D-F) Analysis of polyclonal CD4^{+} T cells and *Ct*-STL reactive RG1-expressing T cells in the SILP of cDC subset-deficient mice (expt.=2). 10^{5} retrovirally-transduced RG1 T cells were transferred 3 days after *Ct*-STL colonization, and assessed

after 1 week for transcription factor expression by intracellular staining. FACS plots are representative of high FoxP3 and RORγt mice. Each dot represents data from an individual host. Geometric mean ± geometric S.D. (A) or mean ± S.E.M. are shown. Repeated measures mixed effects analysis (A, B left) or ANOVA with Dunnett's correction (B right, C-F) p-values are shown.

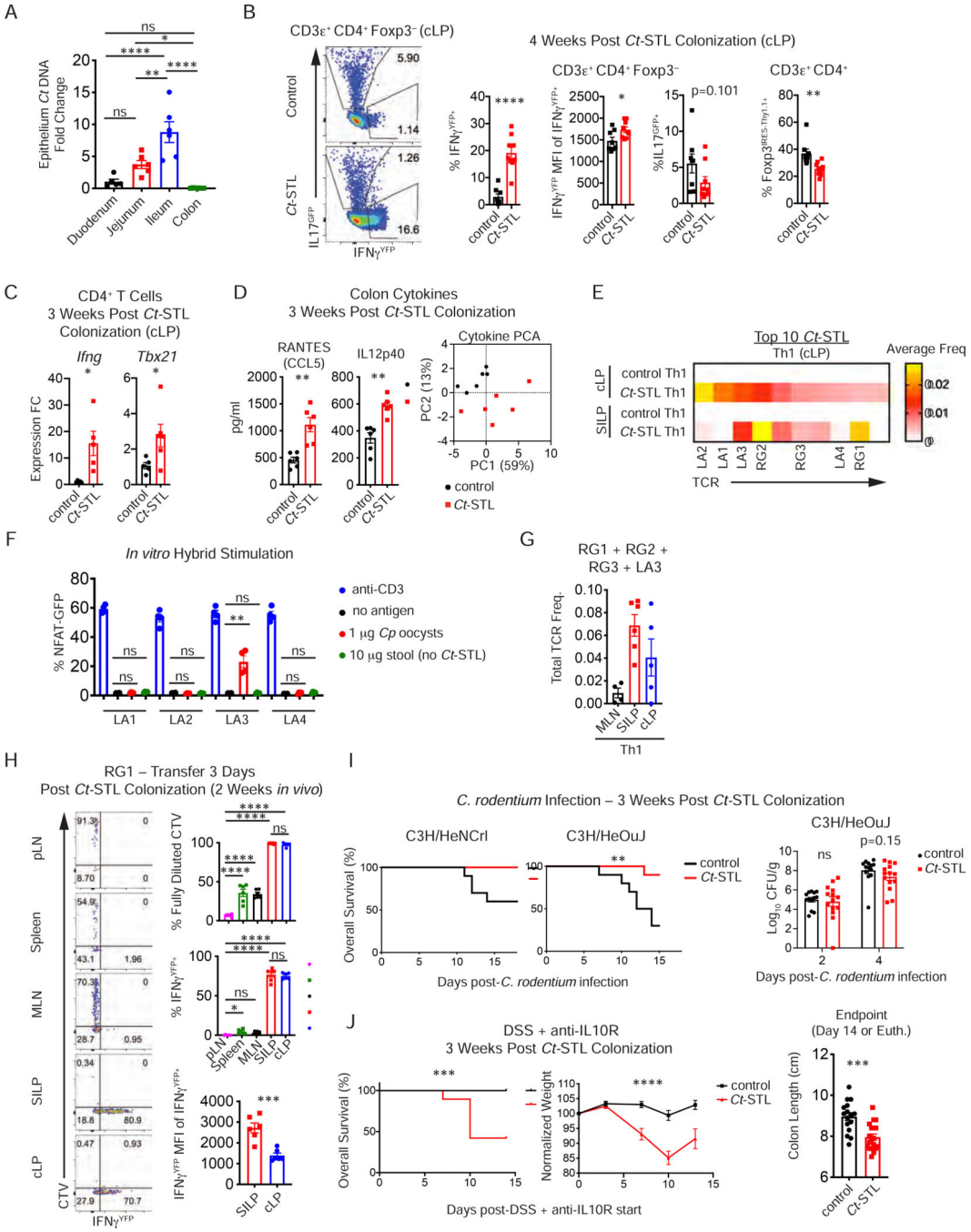

Figure 7. Homeostatic *Ct*-STL induces colon Th1 responses and facilitates immunity to pathogens

(A-D) Analysis of mice 3 weeks after colonization with *Ct*-STL at weaning. (A) Relative quantification of *Ct*-STL *Gapdh* to mouse *Trac* DNA in different segments of intestinal epithelium in mice 3 weeks after Ct-STL colonization. *Ct Gapdh* fold change is normalized to the average of all samples. (expt.=2). (B-C) IFNγ expression in cLP polyclonal CD4$^+$ T cells by (B) flow cytometry of IFNγ^{YFP} IL17^{GFP} Foxp3$^{Thy1.1}$ mice (expt.= 3) or (C) qPCR of sorted CD4$^+$ T cells for *Ifng* and *Tbx21* expression (expt.=2). (D) Cytokine analysis of colons by multiplex Luminex assay. PCA using RANTES, IL12p40, and Figure S7G

cytokines is displayed (expt.=2). (E) Comparison of the top 10 colon Th1 TCRs vs SILP TCRs in *Ct*-STL colonized mice (see also Figure 5, expt.=5). TCRs tested are indicated (n=5 for *Ct*-STL cLP, n=3 for control cLP, n=5–6 for SILP). (F) *In vitro* reactivity of *Ct*-STL-colonized colon Th1 TCRs shown in (E) to *Cp* oocyst antigens as per Figure 4D (expt.=2). (G) Cumulative frequencies of known *Ct*-STL-reactive TCRs in the MLN, SILP, and cLP Th1 TCR repertoires at homeostasis. (H) 2×10^5 retroviral RG1-expressing IFNγ^{YFP} TCli-β T cells were transferred into 3.5-week-old CR WT mice 3 days after *Ct*-STL colonization, and analyzed for CTV dilution and IFNγ^{YFP} expression after 2 weeks in the pLN (axillary, inguinal, and brachial), spleen, MLN, SILP, and cLP. (expt.=2). (I) *C. rodentium* infection of 2 strains of C3H from 2 different vendors 3 weeks after colonization at 3.5 weeks of age. Survival is based on euthanasia at 20% weight loss (n=10 per group, expt.=2 per C3H strain). *C. rodentium* CFUs in stool are shown (right, expt.=3). (J) Colon injury in DSS and anti-IL10R-treated, *Ct*-STL-colonized and control mice. 3.5 week old CR WT mice were colonized with *Ct*-STL as in (I) and then treated with 1 mg of anti-IL10R one time plus 1% DSS in drinking water for 7 days. Survival, weight loss, and colon length at end of experiment or euthanasia threshold (20% weight loss or morbidity) were assessed (n=16–19 per group, expt.=3). Each dot represents data from an individual host (A-D, G-H, I right, J right) or individual hybrid experiment well (F). Mean ± S.E.M. error bars are shown. Student's t-test (B-C, H bottom, J right), Kaplan-Meier (I, J), one-way ANOVA with Dunnet's (F) or Sidak's (H) correction, Mann-Whitney test (I right), or repeated measures mixed effects analysis (J middle) p-values are shown. Multiple t-tests with FDR-correction (Benjamini, Krieger, and Yekutieli) q-values are shown in (D).

KEY RESOURCES TABLE

REAGENT or RESOURCE	SOURCE	IDENTIFIER
Antibodies		
anti-IFNγ Clone H22	Leinco	Cat#I-438
PIP	Leinco	Cat#P-376
anti-Thy1.2 clone 30H12	BioXCell	Cat#BE0066
LTF-2	BioXCell	Cat#BE0090
anti-NK1.1 clone PK136	BioXCell	Cat##BE0036
C1.18.4	BioXCell	Cat#BE0085
anti-IL10R	BioXCell	Cat#BE0050
anti-CD3ε	BioXCell	Cat#BE0001-1
anti-MHCII	BioXCell	Cat#BE010
anti-CD28	BioXCell	Cat#BE0015-1
anti-TGFβ	BioXCell	Cat#BE0057
anti-IL-12	BioXCell	Cat#BE0052
anti-IFNγ	BioXCell	Cat#BE0054
anti-IL-4	BioXCell	Cat#BE0045
Anti-mouse CD3ε (clone#145-2C11) FITC, PE, and BV421	BioLegend	Cat#100305/07/35
Anti-mouse/human B220 (clone#RA3-6B2) APC/Cy7, A700, and PE/Cy7	BioLegend	Cat#103223/31/22
Anti-mouse CD19 (clone#6D5) APC/Cy7	BioLegend	Cat#115529
Anti-mouse I-Ab (clone#AF6-120.1) APC and PerCP/Cy5.5	BioLegend	Cat#116417/15
Anti-mouse CD11c (clone#N418) PE/Cy7 and BV605	BioLegend	Cat#117317/33
Anti-mouse/human CD11b (clone#M1/70) BV711	BioLegend	Cat#101241
Anti-mouse CD103 (clone#2E7) BV421	BioLegend	Cat#121421
Anti-mouse F4/80 (clone#BM8) PE/Cy7	BioLegend	Cat#123113
Anti-mouse CD4 (clone#RM4-5) BV711, PE, PB, and BV605	BioLegend	Cat#100549/11/34/48
Anti-mouse CD25 (clone#PC61) APC, BV605, PerCP/Cy5.5, and PE/Cy7	BioLegend	Cat#102011/35/29/15
Anti-mouse/human CD44 (clone#IM7) APC/Cy7 and BV605	BioLegend	Cat#103027/47
Anti-mouse CD62L (clone#MEL-14) APC/Cy7 and BV605	BioLegend	Cat#104427/37
Anti-mouse FOXP3 (clone#FJK-16s) FITC	ThermoFisher	Cat#11-5773-82
Anti-mouse GATA3 (clone#16E10A23) PE	BioLegend	Cat#653803
Anti-mouse RORγt (clone#B2D) APC	ThermoFisher	Cat#17-6981-80
Anti-mouse TBET (clone#4B10) PE/Cy7	BioLegend	Cat#644823
Anti-mouse CXCR3 (clone#CXCR3-173) BV421, PE, and APC	BioLegend	Cat#126521/06/12
Anti-mouse Thy1.1 (clone#OX-7) BV711, PE/Cy7, and PerCP/Cy5.5	BioLegend	Cat#202539/18/16

REAGENT or RESOURCE	SOURCE	IDENTIFIER
Anti-mouse CD80 (clone#16-10A1) APC	BioLegend	Cat#104713
Anti-mouse CD45.1 (clone#A20) PerCP/Cy5.5, PE, and A700	BioLegend	Cat#110728/08/24
Anti-mouse CD45.2 (clone#104) APC, A700, and PE	BioLegend	Cat#109814/22/08
Anti-mouse VB6 (clone#RR4-7) PE and APC	BioLegend	Cat#140003/5
Anti-mouse VB5 (clone#MR9-4) PE	BioLegend	Cat#139503
Anti-mouse Va2 (clone#B20.1) APC/Cy7 and PerCP/Cy5.5	BioLegend	Cat#127818/14
Bacterial and virus strains		
Citrobacter rodentium	Gift from M. Colonna (Wash. U.)	
Biological samples		
Cryptosporidium tyzzeri (*Ct*-STL)	Our mouse colony	N/A
Chemicals, peptides, and recombinant proteins		
FITC-Dextran	Sigma	Cat#FD4
Ovalbumin (Grade V)	Sigma	Cat#A5503
Incomplete Freund's Adjuvant	Sigma	Cat#F5506
Ovalbumin (Grade VI)	Sigma	Cat#A2512
Dextran Sodium Sulfate	TdB Labs	Cat#9011-18-1
Critical commercial assays		
Quick-DNA Fecal/Soil Microbe Prep Kit	Zymo	Cat#D6010
Luminaris Color HiGreen qPCR Master Mix	ThermoFisher	Cat#K0391
CountBright Absolute Counting Beads	ThermoFisher	Cat#C36950
Crypt-a-Glo	Waterborne	Cat#A400FLR
TransIT-293	ThermoFisher	Cat#MIR2700
CellTrace Violet (CTV)	ThermoFisher	Cat#C34571
SuperScript III Reverse Transcriptase	ThermoFisher	Cat#18080093
Accuzyme DNA Polymerase	Bioline	Cat#BIO-21052
Foxp3/Transcription Factor Staining Buffer Set	ThermoFisher	Cat#00-5523-00
Bio-Plex Mouse Cytokine 23-plex Assay	BioRad	Cat#M60009RDPD
Deposited data		
TCR Sequencing	This paper	ENA: accession #PRJEB46540
16S rRNA	This paper	ENA: accession #PRJEB46540
Experimental models: Cell lines		
NFAT-GFP T cell hybridoma	Gift from K. Murphy (Wash. U.) (Ise et al., 2010)	N/A
B16 flt3L melanoma	Gift from G. Dranoff (Mach et al., 2000)	N/A
Experimental models: Organisms/strains		
Mouse: C57BL/6-Ly5.1	Charles River	Cat#494
Mouse: C57BL/6NCrl (Ly5.2)	Charles River	Cat#027
Mouse: C57BL/6J	JAX	Cat#000664
Mouse: *Rag1*$^{-/-}$	JAX	Cat#002216

REAGENT or RESOURCE	SOURCE	IDENTIFIER
Mouse: hLang^{DTA}	Gift from D. Kaplan (U. Pitt.) (Kaplan et al., 2005)	N/A
Mouse: *Irf8* +32 5'$^{-/-}$	Gift from K. Murphy (Wash. U.) (Durai et al., 2019)	N/A
Mouse: Foxp3$^{IRES-GFP}$	JAX	Cat#006772
Mouse: Foxp3$^{IRES-Thy1.1}$	Gift from A. Rudensky (MSKCC) (Liston et al., 2008)	N/A
Mouse: IL-17A$^{IRES-GFP}$	JAX	Cat#18472
Mouse: IL12p40$^{IRES-YFP}$	JAX	Cat#015864
Mouse: *Ifngr1*$^{-/-}$	JAX	Cat#003288
Mouse: C3H/HeOuJ	JAX	Cat#000635
Mouse: IFNγ$^{IRES-YFP}$	Gift from R. Locksley (UCSF) (Reinhardt et al., 2009)	N/A
Mouse: TCli TCRβ Transgenic	Gift from A. Rudensky (MSKCC) (Wong et al., 2000)	N/A
Mouse: TCli TCRαβ Transgenic	Gift from A. Rudensky (MSKCC) (Wong et al., 2000)	N/A
Mouse: *Tcra*$^{-/-}$	Jax	Cat#002116
Mouse: C3H/HeNCrl	Charles River	Cat#025
Mouse: OT-II Transgenic	JAX	Cat#004194
Oligonucleotides		
Primers for TCR-seq, see Table S1	N/A	N/A
Other primers, see Table S5	N/A	N/A
Recombinant DNA		
(RG1/RG2/RG3/LA1/LA2/LA3/LA4/CT6)-IRES-Thy1.1	This paper and (Hsieh et al., 2004; Lathrop et al., 2011)	N/A
RG1-P2A-Akaluc	This paper and (Iwano et al., 2018)	N/A
CT2-P2A-Akaluc	This paper and (Iwano et al., 2018)	N/A
Software and algorithms		
Prism v9	https://www.graphpad.com	N/A
FlowJo v10	https://www.flowjo.com	N/A
ImageJ v1.53a	https://imagej.nih.gov/ij/download.html	N/A
MegAlign v16	https://www.dnastar.com	N/A
R	https://www.r-project.org/	N/A
dada2 v1.14	https://www.bioconductor.org/packages/release/bioc/html/dada2.html	N/A
Vegan v2.4	https://cran.r-project.org/web/packages/vegan/index.html	N/A
Phyloseq v1.32	https://www.bioconductor.org/packages/release/bioc/html/phyloseq.html	N/A
DESeq2 v1.28	https://bioconductor.org/packages/release/bioc/html/DESeq2.html	N/A
Gbm v2.1	https://cran.r-project.org/web/packages/gbm/index.html	N/A